Alma Mater Studiorum – Università di Bologna

DOTTORATO DI RICERCA IN

Ingegneria Ambientale, Civile e dei Materiali

Ciclo XXVIII

**Settore Concorsuale di afferenza:** 08 A2

**Settore Scientifico disciplinare:** ING/IND 30

TITOLO TESI

# *Numerical modelling and simulation optimization of geothermal reservoirs using the TOUGH2 family of codes*

**Presentata da:** ***Ester Maria Vasini***

**Coordinatore Dottorato** — ***Prof. Alberto Lamberti***

**Relatore** — ***Prof. Villiam Bortolotti***

**Correlatore** — ***Ing. Alfredo Battistelli***

**Esame finale anno 2016**

# Abstract

In order to improve the reservoir engineering activities and, in particular, to optimize numerical modelling and simulation of geothermal reservoirs using the TOUGH family of codes, it has been decided to use the software T2Well for the interpretation of well-tests, coupling T2Well with the equation of state module EWASG, which describes the typical thermodynamic condition in high enthalpy geothermal reservoirs. T2Well-EWASG has been coupled and tested through the typical process of verification and validation. The application of T2Well-EWASG for the interpretation of well-tests related to the slim hole WW-01 drilled in the Wotten Waven Field (Commonwealth of Dominica) proves that it can be used as a tool for integrated interpretation of surface and downhole measurements collected during the performance of production tests in geothermal wells. The strength of this tool is that it allows to reduce the different possible solutions (in terms of reservoir characterization) within an acceptable error, by allowing the interpretation of surface and downhole measurements in conjunction, instead of separately. From this point of view T2Well-EWASG can effectively be used as a tool which allows an improvement of reservoir engineering activities. Finally, the huge amount of data managed during these activities has permitted to test and project the improvement of pre- and post- processing tools specific for TOUGH2 created by the geothermal research group of DICAM. In particular, the pre- and post-processing tools have been validated with a case study dealing with the migration of non-condensable gases in deep sedimentary formation.

# Contents

# Nomenclature

| | | |
|---|---|---|
| $A$ | *Cross sectional area* | $m^2$ |
| $b_0$, $b_1$, $b_2$ | *Constant coefficients* | |
| $b_3$, $b_4$ | *Polynomial function of the temperature* | |
| $C$ | *Specific heat* | $J°C^{-1}kg^{-1}$ |
| $C_0$ | *Profile parameter* | |
| $d$ | *Wellbore diameter* | $m$ |
| $D$, $D_1$ | *Salt concentration polynomials* | |
| $E_0$, $E_1$, $E_2$, $E_3$, $E_4$ | *Pressure dependent coefficient* | |
| $\vec{F}$ | *Mass or energy flux* | $kg\ m^{-2}s^{-1}$ or $J\ m^{-2}s^{-1}$ |
| $f$ | *Fanning friction factor* | |
| $g$ | *Gravitational acceleration* | $m\ s^{-2}$ |
| $h$ | *Specific enthalpy* | $J\ kg^{-1}$ |
| $j$ | *Volumetric flux* | $(m^3s^{-1})m^{-2}$ |
| $k$ | *Absolute permeability* | $m^2$ |
| $k_r$ | *Relative permeability* | |
| $l$ | *Temperature dependent parameter* | |
| $M$ | *Mass or energy per volume* | $kg\ m^{-3}$ or $J\ m^{-3}$ |
| $NEL$ | *Number of grid blocks* | |
| $NEQ$ | *Number of equation* | |
| $NK$ | *Number of mass components* | |
| $P$ | *Pressure* | $Pa$ |
| $PM$ | *Molecular weight* | *Atomic mass unit* |
| $q$ | *Mass or energy generation rate* | $kg\ m^{-3}\ s^{-1}$ or $J\ m^{-3}\ s^{-1}$ |
| $R$ | *Residuals* | |
| $r$ | *Radius* | $m$ |
| $Re$ | *Reynolds number* | |

| | | |
|---|---|---|
| $S$ | *Saturation* | |
| $T$ | *Temperature* | $°C$ |
| $t$ | *Time* | $s$ |
| $t_D$ | *Dimensionless time* | |
| $u$ | *Specific internal energy* | $J\ kg^{-1}$ |
| $U$ | *Over-all heat transfer coefficient* | $W°C^{-1}\ m^{-2}$ |
| $V$ | *Volume* | $m^3$ |
| $v$ | *Velocity* | $m\ s^{-1}$ |
| $X$ | *Mass fraction* | |
| $y$ | *Heat transfer coefficient* | $W\ °C^{-1}\ m^{-2}$ |
| $Z$ | *Set of n points* | |

## Greek letters

| | | |
|---|---|---|
| $\alpha$ | *Halite solubility* | |
| $\Gamma$ | *Surface area* | $m^2$ |
| $\gamma$ | *Euler costant* | |
| $\delta$ | *Euclidean distance* | |
| $\varepsilon$ | *Roughness* | |
| $\theta$ | *Angle between wellbore section and vertical direction* | |
| $\lambda$ | *Thermal conductivity* | $W\ °C^{-1}m^{-1}$ |
| $\mu$ | *Dynamic viscosity* | $Pa{\cdot}s$ |
| $\rho$ | *Density* | $Kg\ m^{-3}$ |
| $\tau$ | *Shear stress* | |
| $\phi$ | *Porosity* | |

## Subscript

| | |
|---|---|
| $c$ | *Natural conduction* |
| $cem.$ | *Cementation* |
| $ci$ | *Inner casing* |

| | |
|---|---|
| *co* | *Outer casing* |
| *D* | *Dimensionless* |
| *E* | *Formation* |
| *f* | *Film* |
| *G* | *Gas phase* |
| *h* | *Outer cementation* |
| *i* | *$I^{th}$ element or grid block* |
| *L* | *Liquid phase* |
| *m* | *$M^{th}$ element or mixture* |
| *n* | *$N^{th}$ element* |
| *r* | *Radiation* |
| *R* | *Rock* |
| *ti* | *Inner tubing* |
| *to* | *Outer tubing* |
| *tub.* | *Tubing* |
| *w* | *Wellbore* |
| *β* | *Phase (liquid or gas)* |

Superscript

| | |
|---|---|
| *k* | *Number of equations [k=1, 2, …, NEQ; NEQ=NK+1]* |
| κ *and* κ*+1* | *Time steps* |

# List of Figures

# List of Tables

# Acknowledgements

I would like to thank the Geothermal Project Management Unit (PMU) of the Commonwealth of Dominica and ELC Electroconsult SpA for the permission to use well WW-01 field data.

Furthermore I would like to thank all the people who helped me with suggestions and inspirations: the Geothermal Research group of DICAM, Prof. Villiam Bortolotti, Prof. Paolo Berry, PhD Eng. Stefano Bonduà and PhD Eng. Carlo Cormio; Eng. Alfredo Battistelli of Saipem SpA, who collaborated to this work under the R&D project "Simulation of production tests with TOUGH2-T2Well", and PhD Lehua Pan of the Lawrence Berkeley National Laboratory.

# Introduction

In the last few decades, the demand of environmentally friendly energy is felt stronger. For “environmentally friendly energy” is meant the use of sources of energy not only less polluting, but also sustainable and renewable [Axelsson and Stefansson, 2003]. Geothermal energy, if correctly produced and managed, is one of these, and it is characterized by a particular versatility. In fact, it is used not only for the production of electrical energy (with temperature higher than approximately 150°C), but also in the case of lower temperature systems suitable for direct heat uses, such as space heating/cooling, greenhouses, aquaculture, etc. Italy was the first country in the world to develop the technology for the exploitation of geothermal energy (by Prince Piero Ginori Conti, 1904) and it is currently one of the world leaders in terms of electricity production from geothermal sources [Notiziario UGI, 2007; Bertani, 2015].

One of the goals concerning the geothermal exploitation activities is to keep the resource alive/available as much as possible, thus keeping the extraction of geothermal fluids compatible with the reservoir recharge, and taking advantage of the re-injection of the extracted fluids. During the exploitation of a geothermal reservoir it is therefore mandatory to be able to correctly plan the field development and perform a sound management of fluids production. This is a challenging activity that nowadays is essentially accomplished using numerical reservoir simulation. Geothermal numerical simulators, therefore, are of paramount importance to optimize the exploitation, for the

characterization of geo-resources, to evaluate the economic sustainability of the project and estimate the environment impact.

It is, therefore, easy to understand that any effort dedicated to the improvement and optimization of numerical modelling and simulation is welcome, and this is the main objective of this study, particularly regarding the TOUGH family of codes [Pruess, 2004; Finsterle et al., 2014].

During the doctoral research work, many aspects of the geothermal numerical modeling and simulation were tackled and many specific software tools were used. In particular the improvement of the reservoir engineering activities has been a central point of the doctoral work. The main research work, therefore, deals with the use and improvement of T2Well (a coupled well-reservoir simulator based on TOUGH2, [Pan and Oldenburg, 2013] ) for the interpretation of geothermal well-tests. The dynamic P&T (pressure and temperature) logs and the pressure transient measurement during well-tests, unfortunately, are often incomplete, both for time saving and for issues related to the risk of loss of the logging tools, and this is a strong limitation in understanding of the reservoirs characteristics. A good way to solve the lack of these downhole data may be the use of coupled wellbore-reservoir flow simulation under transient conditions. In this way, it is possible to interpret the well-tests by means of simulations which allow analyzing the bottom and well-head measurements in an integrated approach, instead of analyzing them separately [Battistelli, 2016]. This can be done using, for instance, T2Well coupled with a proper Equation of State (EOS) module in order to allow the simulation of commonly exploited geothermal systems. While EWASG can be conveniently used to simulate geothermal reservoirs with temperatures from low to high, the applications described here below were focused on high temperature (or high enthalpy) reservoirs used for the generation of electrical energy. As high enthalpy geothermal fluids consist of mixtures of water, salts and non-condensable gases, supported by Eng. A. Battistelli and PhD L. Pan, T2Well was coupled with the EWASG module [Battistelli et al., 1997; Battistelli, 2012] to create the new code called

T2Well-EWASG. Furthermore, the analytical approach for the computation of heat exchange between the wellbore and the formation (option included in T2Well) was enhanced. The verification of T2Well-EWASG was accomplished by comparing analytical and numerical results concerning the heat exchange between the wellbore and the formation. The validation was obtained by reproducing flowing pressure and temperature logs taken from published literature and by using T2Well-EWASG for the interpretation of a short production test, performed on an exploratory well drilled in a recently discovered geothermal field.

Another important activity carried on during the doctoral work, concerns the improvement of pre- and post- processing tools specific for TOUGH2. Many efforts were done to modify the viewer TOUGH2Viewer [Bonduà et al., 2012] to work in conjunction with VORO2MESH [Bonduà et al., 2015]. In particular, TOUGH2Viewer was improved with new functionalities allowing managing fully unstructured 3D Voronoi grids created with VORO2MESH. The viewer was validated with a case study dealing with the migration of non-condensable gases in a deep sedimentary formation [Battistelli et al., 2015] using TOUGH2-TMGAS [Battistelli and Marcolini, 2009].

The thesis is structured as follows: It starts with a background chapter, where the topic of the research is described. Chapter 2 describes the TOUGH and T2Well software and the pre- and post-processor VORO2MESH and TOUGH2Viewer. Chapter 3 describes the T2Well-EWASG development and modifications; in chapter 4 the results of verification and validation of the software are provided. In chapter 5 the results of the application of TOUGH2Viewer and VORO2MESH are shown. Finally in chapter 6 conclusions and the hypothesis on future developments of the research are discussed.

# 1 Background

## 1.1 System, model, calibration and simulation

Defining the term *process* as a set of interactions, energy or material transformations and transmissions, aimed to obtain a certain goal, it is possible to define the system as a conglomerate of parts through which the process is realized. In other words, a *system* is a set of interacting parts, which constitute a single "body", and that permits to the *process* to occur. The system behavior is characterized by a set of properties, which can be divided into two categories: the *parameters*, which usually are invariant system characteristics through time, and the *variables*, which are changing through the time as a consequent of the interactions between the different parts of the system and with the world external to the system. Usually, a real system is very difficult to analyze and study, because of the inability to proper evaluate the numerous system properties. For this reason, typically, the system is not studied directly, but using its simplified version which exclusively includes the crucial aspects of the system that concerns the problem analyzed. This simple version of the system is called *model*. There are different types of models: physical model, which can be scale models (scale representation of each element of the system) or analog model (representation of the system properties through different physical quantities), symbolic models (system representation in terms of symbols, which can be manipulated). The mathematical models, which describe the system in terms of equations and functional relations, are an example of symbolic models and can be

distinguished in two categories: *analytical* and *numerical* models. The analytical models provide exact solutions, if any. The numerical models produce approximate solutions which are reasonably close to the expected results. Since in many cases it is impossible to obtain a solution of the analytical equations the numerical models are the only way to proper represent the system. As state before, the models are used in order to analyze and study the system, but in particular they allow two actions: the interpretation and the simulation. The *interpretation* is the procedure to interpret the output data of the system obtained by a specific stimulation of the system itself. The interpretation, therefore, is used in very important activities such as model calibration in primis, and in some extent also in sensitivity analysis and in the analysis of error propagation. In particular, the *model calibration* allows to obtain the better values of the parameters of the model (that also are parameters of the system) such that the model behavior is in agreement with that of the system. The *sensitivity analysis* allows to individuate what the parameters of the model are whose variations mostly impact on the output behavior of the model itself. Finally, the study of *error propagation* permits to evaluate the influence of the uncertainty of the parameters on the model results. The *simulation* is an activity which allows to use the model in order to obtain information about the behavior of the system, both in the original state evolution (natural state, before the exploitation of the system starts) and in its future evolution (during the exploitation period) [Bortolotti, 2013].

## 1.2 Numerical reservoir simulation

The multiphase multicomponent transport of mass and energy in porous and fractured rocks can be described by a set of partial differential mass and energy balance equations for which closed analytical solutions exist only for very simplified geometries, rock property distribution and thermodynamic

conditions. Thus, the set of partial differential equations suitable to describe the multiphase flow in geothermal reservoirs need to be solved with a numerical approach, by discretizing in space and time the partial differential equations in order to obtain an equivalent system of linear algebraic equations, which can then be solved with direct or iterative approaches. The numerical solution of complex differential equations becomes feasible with the diffusion of digital computers in the late 1960s. First adopted by the oil and gas industries, the numerical simulation becomes a common tool for the geothermal industry in the ‘80s. With the growth of computational power, the models gradually became more sophisticated, starting from very simple models, limited in details and characterized by, for example, single layer structure or 2D geometry, to achieve very detailed models, characterized, for example, by mesh with more than $10^6$ grid blocks and layers that follow the geological structure of the formation [O’Sullivan et al., 2001].

Numerical modelling and simulation of geothermal reservoirs are essential tools in order to better optimize the resource exploitation and characterization. In fact, the simulation permits not only to study the reservoir before exploitation (i.e. the natural state modelling, that provides information that serve as the basis for exploitation models that may later be developed) but also to predict the possible future exploitation scenarios. The simulation is also useful to test the number and location for the wells, based upon a given generating capacity, to predict the longevity of the field according to a defined exploitation plan and to realize sensitivity studies [Bodvarsson, 1982].

Basically the numerical simulation consists in these main activities:

1. Collection of data, coming from geosciences, well production and reservoir engineering;
2. Review and interpretation of field data;
3. Development of the conceptual model;
4. Building of the numerical model;
5. Natural state calibration (by trial-and-error or with inverse simulation techniques);

6. Matching of production history (by trial-and-error or with inverse simulation techniques);
7. Forecast of production and reinjection scenarios;

The first step involves the collection of all the needed data about the system in order to develop a conceptual model of the field. Collection and interpretation of field data is performed by experts in geosciences (geology, geophysics, geochemistry), taking advantage of both surface surveys and drilled wells, as well as by experts in well production and reservoir engineering. The construction of the conceptual model is a prerequisite of the simulation process because it is an outline that tries to connect all the available and useful information about the system and it requires the consultation of wide range of expertise: geologists, chemists, reservoir engineering and physicists [Grant M.A., Bixley P.F., 2011, cap 11]. Once the conceptual model has been developed, it is translated into the numerical model, in a format acceptable by the simulator (the software). Once the numerical model has been developed, it is possible to simulate the natural state condition. The simulation starts and goes on until the achievement of steady state conditions, which are usually assumed to be a proxy for the natural state. The natural state calibration consists in the adjustment of the model parameters by comparing the simulation results with the natural state conditions as depicted in the conceptual model, for example by comparing shut-in pressure and temperature profile measured in drilled wells with simulated results. The model parameters are changed until the differences between simulated and experimental data becomes lower than a target threshold. The history matching is performed using production/reinjection data: the model parameters are changed until the simulation results match the recorded behavior under exploitation of the actual reservoir. This last step is very important in order to determine the hydraulic condition of the formation [Grant M.A., Bixley P.F., 2011, cap 11]. De facto the realization of a model which reflect the actual system and that permits to predict different possible

exploration scenarios needs a continuous upgrade of data. Every experimental data, pressure and temperature logs, well test, etc, which become available with time, are important for the determination of the natural state and for the calibration and history matching of the model [Grant M.A., Bixley P.F., 2011, cap 11]. In this terms it can be stated that both the conceptual and numerical models need to be periodically updated during the development and exploitation phases to take advantage of new field observation acquired. Finally, once the model is calibrated, it is possible to use it in order to predict the possible future exploitation scenarios, in the process called forward simulation.

One of the main intent of the modeling activities is the evaluation of the spatial distribution of hydraulic properties and thermodynamic condition of the reservoir. Such characteristics play a key role in determining the production capacity of the wells and the reservoir behavior under exploitation. Common well-tests performed for the evaluation of the hydraulic properties are: production testing, shut-in and flowing temperature and pressure logging (either during injection and production and during and after drilling of the well), down-hole pressure transient measurements. For a more detailed description of the objectives and characteristics of well-test the reader is referred to Grant and Bixley 2011.

Production tests serve for the determination of the fluid enthalpy and to obtain the deliverability curve (flow rate versus the well head pressure). The P&T (pressure and temperature) logs, recorded both during injection and production, allow to locate the feed-zone, the thermodynamic properties of the feed-zone fluids and they are usually used for the calibration of the model. Pressure transient analysis requires the disturbance of the pressure state of the reservoir by production or injection and measuring the resulting pressure transients. They are performed to assess the principal hydrological parameters of the formation near the well, such as [Axelsson, 2013]:

- formation permeability-thickness;
- formation storage coefficient;

- skin factor of the well;
- wellbore storage coefficient.

### 1.2.2 Reservoir Simulators

The first geothermal simulator has been developed in the 1970s for the study of the Wairakei geothermal field [O'Sullivan et al., 2009]. Development of geothermal numerical reservoir simulators at Lawrence Berkeley Laboratory (now LBNL) started in 1975 with the first version of SHAFT [Lasseter et al., 1975] and continued with the SHAFT78 and SHAFT79 release [Pruess, 1988]. In 1977 Faust and Mercer realized a model that can simulate two-dimensional flow of compressed water, two-phase mixture and super-heated steam over a temperature range between 10° and 300°C [Faust and Mercer, 1977]. In 1982 Bodvarsson realized PT (pressure-temperature) a simulator for three-dimensional mass and energy transport in a liquid-saturated medium, based on Integrated Finite Difference Methods (IFDM). PT also computes the deformation of the medium using the one-dimension consolidation theory of Terzaghi [Bodvarsson, 1982]. AQUA [Hu S., 1994; Hu B., 1995] is a software developed by Vatnaskil Consulting Engineers, 1990, to modelling the groundwater fluid flow and transport, based on the Galerkin finite element method. Aqua3D is a Galerkin finite-element numerical modelling software used to model 3D groundwater and contaminant transport, sell by Vatnaskil consulting engineers since 1997 [Vatnaskil, 1997]. HYDROTHERM [Hayba and Ingebritsen, 1994] is a finite-difference model describing three-dimensional, multiphase flow of pure water and heat at near-critical and supercritical temperatures (up to 1200°C). It has been developed as an extension of multiphase geothermal models produced by Faust and Mercer in the 1970s. This kind of multiphase model are needed in study related cooling plutons, crustal-scale heat transfer and volcanic systems with shallow intrusion.

Common simulators are STAR [Pritchett, 1995], a simulator for multiphase, multicomponent transport of fluid mass and heat in three-dimensional geologic media, and TETRAD [Vinsome and Shook, 1993], which require regular rectangular meshes. In this work was used one of the most popular software for geothermal numerical modeling, TOUGH2 [Pruess et al., 1999].

#### 1.2.2.1 Brief overview on TOUGH family of codes

TOUGH is an acronym, which stand for "Transport Of Unsaturated Groundwater and Heat". The most famous software of the TOUGH family of codes is TOUGH2. TOUGH2 is a numerical simulator for non-isothermal flows of multicomponent, multiphase fluids in one, two, and three-dimensional porous and fractured media. In addition to being widely used for geothermal simulations, TOUGH2 is used also for modelling of nuclear waste disposal, environmental remediation and geological carbon storage. TOUGH2 is used not only for academic purpose but also for private industrial works and also by government organization [Finsterle et al. 2014]. TOUGH2 is the result of about forty years of research at the Lawrence Berkeley National Laboratory (LBNL). After SHAFT, the first prototype developed in mid '70s [Pruess, 1988], in the 1980s, LBNL developed MULKOM, a modular architecture for simulating the flow of multicomponent, multiphase fluids and heat in permeable (porous or fractured) media [Pruess, 2004]. In 1987 a specialized version of MULKOM was released to the public under the name of TOUGH [Pruess, 1987], that was able to handle two-phase flow of water-air mixture. Subsequently, in 1991 TOUGH2 [Pruess, 1991], a more global set of MULKOM modules, was released, followed by TOUGH2 version 2.0 [Pruess et al., 1999] in 1999. Unlike STAR and TETRAD, TOUGH2 is able to handle unstructured meshes. TOUGH2 is structured by a modular architecture: there is a core module dedicated to assemble and

iteratively solve the flow equations and an Equation Of State (EOS) module, which is dedicated to the description of the specific thermophysical properties of fluid mixtures involved in the problems.TOUGH2 V.2.0 is written in FORTRAN 77 and requires as input a set of ASCII files (whose manipulation is not easy without specific pre-processor software, especially in the case of full field simulations) defining the numerical model and its use in the simulation process. A more detailed description of TOUGH2 is proposed in chapter 2.

Other relevant tools from the TOUGH family of codes are T2VOC [Falta et al., 1995] and TMVOC [Pruess and Battistelli, 2002] and TMVOCBio [Battistelli, 2004] dedicated to study environmental contamination problems in presence of non-aqueous phase liquids. TOUGHREACT [Xu and Pruess, 2001, Xu et al., 2004] was realized for the modeling of non-isothermal multiphase flow and geochemical transport (reactive transport including equilibrium and kinetic mineral dissolution and precipitation, chemically active gases, intra-aqueous and sorption reaction kinetics and biodegradation). iTOUGH2 is an extension of TOUGH2 that allows inverse modeling, parameter estimation, sensitivity analysis, and uncertainty propagation analysis [Finsterle, 2007]. TOUGH-FLAC [Rutqvist et al., 2002] is the coupling of TOUGH2 and FLAC3D [Itasca Consulting Group Inc., 1997] and it allows the integrating simulation of geomechanics deformations and fluid and heat flow in porous media. TOUGH-MP [Zhang et al., 2008] is the TOUGH2 version for the massively parallel computing. TOUGH+ v1.5 [Moridis and Pruess, 2014] is a TOUGH2 successor, which uses dynamic memory allocation and is coded in FORTRAN 95/2003. TOUGH 2.1 [Pruess et al. 2012] is the last version of TOUGH2, with a restructured core, several bug fixes and support to additional EOS modules such as T2VOC, EOS7CA, ECO2N, ECO2M, and TMVOC.

#### 1.2.2.2 Pre- and Post-processing tools for TOUGH family of codes

As mentioned in the previous section, TOUGH2 does not have a native Graphical User Interface (GUI), so over time many efforts have been spent in order to manage input and output file, both by software houses and by scientific research group. A list of software tools developed by scientific group is: MulGeom [O'Sullivan and Bullivant, 1995], GeoCad [Burnell et al., 2003], G*Base [Sato et al., 2003], Simple Geothermal Modelling Environment [Tanaka and Itoi, 2010], TOUGHER [Li et al., 2011], PyTOUGH [Croucher, 2011; Wellmann et al., 2012]. Whereas a commercial list is: Petrasim [Alcot et al., 2006], WinGridder [Pan, 2003], mView [Avis et al., 2012] and Leapfrog [Newson et al., 2012]. In order to better manage the information required to realize the input files and to easily realize locally refined Voronoi grid, the geothermal research group of DICAM has realized TOUGH2GIS [Berry et al., 2014] a GIS-based pre-processor, and TOUGH2Viewer [Bonduá et al., 2012], a 3D visualization and post-processing tool, recently improved to visualize fully Voronoi 3D grid. To create fully Voronoi [Voronoi, 1908; Aurenhamer, 1991] 3D grids the geothermal research group of DICAM has developed VORO2MESH [Bonduá et al., 2015] a new software coded in C++, based on the voro++ library [Rycroft, 2009].

### 1.2.3 Coupled Wellbore-Reservoir Simulators

Since the 1980s, many efforts have been made in order to couple wellbore and reservoir simulators. The importance of the simulation of coupled wellbore-reservoir fluid flow lies in the fact that the flow inside the geothermal well cannot be considered isolated, but it must be considered in

conjunction with the flow of fluid in the reservoir [DiPippo, 2008]. This approach leads to a more reliable modelling of the phenomena involved in the exploitation of the resource.

One of the first coupled software is due to Miller (1980), who developed a transient-wellbore code, WELBORE. The code allows the simulation of one-dimensional, two-phase, non-isothermal fluid flow in a wellbore coupled with the simulation of single-phase radial flow in the reservoir [Miller, 1980]. Murray and Gunn (1993) proposed a coupled wellbore-reservoir simulator composed by TETRAD and WELLSIM [Gunn and Freeston, 1991; Freeston and Gunn, 1993]. The latest is a steady-state wellbore simulator, which includes three codes: WFSA (for the simulation in presence of dissolved solids, multiple feed-zones and fluid-rock heat exchange), WFSB (dedicated to the simulation of gaseous well) and STFLOW (built to model saturated and superheated steam typical of wellbore located in vapor-dominated zones). TETRAD-WELLSIM coupling works by means of lookup table of wellbore pressure generated by WELLSIM given as input to TETRAD. In a paper of the 1995, Hadgu et al. describe the coupling of TOUGH and the steady-state wellbore simulator WFSA. In this way they were able to model the flow of geothermal brine both in the wellbore and in the reservoir, by using a new module, called COUPLE, which allowed TOUGH to call WSFA as a subroutine. Bhat et al. (2005) coupled TOUGH2 with the steady-state wellbore simulator HOLA [Björnsson, 1987]. HOLA is designed for the modeling of multi-feed zone in a wellbore of pure water, characterized by one or two phase flow. Modified versions of HOLA exist: GWELL, for the modeling of water-carbon mixture and GWNACL for the modeling of water-salt mixture. Similar to the work of Hadgu et al., Bhat et al. integrated HOLA as a subroutine of TOUGH [Bhat et al., 2005]. Tokita et al., presented in 2005 a method developed to predict the effects on a reservoir due to exploitation using a new simulator resulting by the coupling of a reservoir simulator, TOUGH2, a steady-state multi-feed zone wellbore simulator, MULFEWS [Tokita and Itoi, 2004], and a two-phase pipeline network simulator. The

simulator was used to forecast the middle-term power output of the Hatchobaru power plant in Japan. Marcolini and Battistelli [2012] developed wellbore flow modeling capabilities inside TOUGH2 by coding the solution of steady state mass, momentum and energy equations for the wellbore on deliverability option already available in TOUGH2. This code modification, limited to EOS1 and EOS2 modules, was addressed to the modeling of coupled wellbore-reservoir flow in full field geothermal reservoir simulations. Gudmndsdottir et al. (2012) developed a coupled wellbore-reservoir simulator using TOUGH2 and FloWell [Gudmndsdottir et al., 2012; Gudmndsdottir and Jonsson, 2015]. FloWell is a steady-state wellbore simulator dedicated to model liquid, two-phase and superheated steam flows in geothermal wells, and was part of a research project whose aim was to evaluate the well performance and the state of the reservoir using wellhead condition and inverse modeling. To address the need to simulate the coupled wellbore-reservoir flow, Pan and Oldenburg (2013) developed T2Well, a numerical simulator for non-isothermal, multiphase, and multi-component transient coupled wellbore-reservoir flow modeling [Pan and Oldenburg, 2013]. T2Well is the coupled wellbore-reservoir simulator used in this work. T2Well expands the numerical reservoir simulator TOUGH2 capabilities in order to compute the flow in both the wellbore and the reservoir by introducing a special wellbore sub-domain into the numerical grid. The wellbore flow is simulated using the Drift Flux Model [Zuber and Findlay, 1965]. As TOUGH2, T2Well can be used with different EOS in order to describe different fluid mixtures. Up to now it has been used with ECO2N [Pruess, 2005] for applications related to $CO_2$ sequestration [Hu et al., 2012], with ECO2H [Pan et al., 2015] for enhanced geothermal system simulations, with EOS7C [Oldenburg et al., 2013] for applications related to compressed air energy storage, and with EOIL for the modeling of Macondo well blowout [Oldenburg et al., 2011]. The heat exchanges between wellbore and the surrounding formation can be simulated numerically or, alternatively

calculated with the analytical Ramey's method [Ramey, 1962] or the Zhang's convolution method [Zhang et al., 2011].

Since T2Well is simulator, which combine the capabilities and the benefits of TOUGH2 and allows the coupled wellbore-reservoir flow simulation under transient condition, it results that it is the eligible tool for the interpretation of well-tests, allowing the simulation of bottom and well-head measurement in an integrated approach.

A more detailed description of T2Well is proposed in the 2 chapter.

# 2 TOUGH2, T2Well, TOUGH2Viewer and VORO2MESH

## 2.1 TOUGH2

TOUGH2 is a numerical simulator program dedicated to multi-dimensional fluid and heat flow, characterized by multi-component and multiphase fluid mixture, in porous and fractured media. TOUGH2 is widely used in industrial and academic world and in different areas such as geothermal reservoir engineering, radioactive waste disposal, $CO_2$ sequestration, environmental assessment, etc.

TOUGH2 is characterized by a modular structure, with a main module dedicated to the assembling and solution of the flow equation that provides the primary variables to the EOS module and receives from it the values of secondary parameters according to the thermodynamic relation implemented in the EOS module.

There are different EOS modules that describe different thermodynamic systems: EOS1 is dedicated to water and water with tracer, EOS2 describe the thermodynamic equation for a mixture of water and $CO_2$, etc. The available EOS up to now are:

- EOS1: water, water with tracer, heat;
- EOS2: water, $CO_2$, Heat;
- EOS3: water, air, heat;

- EOS4:water, air, with VPL, heat;
- EOS5:water, hydrogen, heat;
- EOS7:water, brine, air, heat;
- EOS7CA: water, brine, NCG ($CO_2$, $N_2$ or $CH_4$), gas tracer, air, heat;
- EOS7R: water, brine, air, parent-daughter radionuclides, heat;
- EOS8: water, air, oil;
- EOS9: Water (Richards'equation);
- T2VOC: Water, air, voc, heat;
- EWASG: Water, salt (NaCl), NCG (includes precipitation and dissolution, with porosity and permeability change; optional treatment of VPL effects), heat;
- ECO2N:water, brine, $CO_2$;
- ECO2M: water, brine, $CO_2$ (multiphase);
- TMVOC: water, VOCs, NCGs;
- T2DM: 2D dispersion module.

This modular structure gives TOUGH2 both the ability to simulate different thermodynamic situations and the flexibility to be applied to different area of interest. The set of primary variables depends on the type of EOS module chosen, for example in EOS2 the primary variables are pressure, temperature and $CO_2$ partial pressure, whereas in EWASG, the primary variables are pressure, salt mass fraction, NCG mass fraction and temperature.

The values of the primary variables are used in the EOS module to compute the secondary parameters, such as density, viscosity, enthalpy, etc. that are used to assemble the mass and energy balance equations.

In the next two paragraphs a survey of the fundamental equation used by TOUGH2 is presented, as it is described by Pruess et al., 1999, in the TOUGH2 v 2.0 manual.

## 2.1.1 Mass and energy balance

For each grid-block of the numerical model, TOUGH2 resolves the mass-energy balance equation:

$$\frac{d}{dt}\int_{V_n} M^k dV_n = \int_{\Gamma_n} \overrightarrow{F^k}\cdot n \; d\Gamma_n + \int_{V_n} q^k dV_n \qquad (2.1)$$

Where $V_n$ and $\Gamma_n$ are respectively the volume and the surrounding surface of the element, $n$ is the normal vector to the surface $d\Gamma_n$ and $F^k$ is the flux term. On the left side of the equation (2.1) there is the accumulation term, $M^k$ that represents the mass (or energy) per volume. On the right side there are two integrals, the first take account of the mass (or heat) flux and the second represents the source and sink contributes. In the mass-case $k = 1, 2, ..., NK$, where $NK$ is the number of mass component. In the case of energy balance $k = NK + 1$.

In the mass balance of a system characterized by more than one component in several phases, the accumulation term takes the form:

$$M^k = \phi \sum_\beta S_\beta \rho_\beta X_\beta^k \qquad (2.2)$$

In which the porosity ($\phi$) is multiplied for the sum of each phase contribute of a k-component. $S_\beta$, $\rho_\beta$ and $X_\beta^k$ are respectively the saturation, the density and the mass fraction of the phase $\beta$. The term, $F^k$, is equal to the sum all over the phases of the flux term of each phase weighted by the mass fraction ($X_\beta^k$):

$$\overrightarrow{F^k} = \sum_\beta X_\beta^k \overrightarrow{F_\beta} \qquad (2.3)$$

Where $F_\beta$ is computed using the Darcy's law:

$$\overrightarrow{F_\beta} = \rho_\beta \vec{v}_\beta = -k \frac{k_{r\beta}\rho_\beta}{\mu_\beta}\left(\nabla P_\beta - \rho_\beta \vec{g}\right) \qquad (2.4)$$

In which compare the Darcy's velocity $\vec{v}_\beta$ of the phase $\beta$, the absolute permeability $k$, the relative permeability $k_{r\beta}$, the viscosity coefficient $\mu_\beta$, the fluid pressure $P_\beta$ related to the phase $\beta$ and the gravity vector $\vec{g}$. In this case the sink and source contribute is a mass rate per volume.

In the energy balance, the heat accumulation is given by two contributes:

$$M^{KN+1} = (1-\phi)\rho_R C_R T + \phi \sum_\beta S_\beta \rho_\beta u_\beta \tag{2.5}$$

The first contribute takes into account the matrix heat provision, $\rho_R$ is the rock density, $C_R$ the rock specific heat and $T$ is the rock temperature. The second contribute stands for the heat of each phase, where $u_\beta$ is the specific internal energy of the phase β.

Heat flux include conductive (Fourier's law) and convective components:

$$\vec{F}^{NK+1} = -\lambda \nabla T + \sum_\beta h_\beta F_\beta \tag{2.6}$$

Where $h_\beta$ is the specific enthalpy of the phase $\beta$, $T$ is the temperature and $\lambda$ is the thermal conductivity.

## 2.1.2 Space and time discretization

TOUGH2 is based on the integral finite difference method (IFDM). Under this point of view, the accumulation term of equation (2.1) becomes:

$$\int_{V_n} M^k dV_n = V_n M_n{}^k \tag{2.7}$$

where $M_n{}^k$ is the average value of $M^k$ in the volume $V_n$ and similarly for the sink and source term:

$$\int_{V_n} q^k dV_n = V_n q_n{}^k \tag{2.8}$$

with $q_n{}^k$ as average mass rate.

The surface integral can be written as:

$$\int_{\Gamma_n} \overrightarrow{F^k} \cdot n \; d\Gamma_n = \sum_m A_{nm} F_{nm} \tag{2.9}$$

In which $F_{nm}$ is the average value of the normal component of the flux $\overrightarrow{F^k}$ to the surface $A_{nm}$ between the element $V_n$ and $V_m$.

In this way, equation (2.1) can be rewritten as:

$$\frac{d}{dt} M_n{}^k = \frac{1}{V_n} \sum_m A_{nm} F_{nm}{}^k + q_n{}^k \tag{2.10}$$

Time is discretized as a first-order finite difference and the flux term is processed with 'fully implicit' method. This means that the flux term and the sink and source contribution, on the right side of equation (2.10), are expressed in terms of the unknown thermodynamic parameters at the time step $t^{\kappa+1} = t^{\kappa} + \Delta t$. This method ensures numerical stability for the calculation of multiphase flow. The time discretization is then represented by the following set of coupled non-linear, algebraic equations:

$$R_n^{k,\kappa+1} = M_n{}^{k,\kappa+1} - M_n{}^{k,\kappa} - \frac{\Delta t}{V_n}\left( \sum_m A_{nm} F_{nm}{}^{k,\kappa+1} + V_n q_n{}^{k,\kappa+1} \right) = 0 \tag{2.11}$$

In which each $R_n^{k,\kappa+1}$ is the residual corresponding to the k[th] equation ($k=1, 2 \ldots NEQ$; $NEQ= NK+1$; $NK$ is the number of fluid components), related to the n[th] element, at the $t^{\kappa+1}$ time step. For each grid block of volume $V_n$ there are NEQ equations. In this way for a system characterized by NEL grid blocks, equation (2.11) represents a set of $NEL \times NEQ$ coupled non-linear equations with $NEL \times NEQ$ unknown independent primary variables which define the state of the flow system at the time step $t^{k+1}$. The resolution of these equations is made using Newton-Raphson iteration.

## 2.1.3 Brief input file description

The TOUGH2 input file is composed by one or more ASCII data files, which describe the rocks properties of the system, the geometry of the mesh, the computational parameters, the initial conditions, etc. All these data have to be provided following a fixed format. The information are organized in blocks, identified by fixed keywords, and up to 80 characters per records compose them (see Figure 1). TOUGH2 adopts the standard metric (SI) unit (meters, seconds, kilograms) with the temperature expressed in Celsius degrees.

```
ROCKS----1----*----2----*----3----*----4----*----5----*----6----*----7----*----8
CAPR1    3     2600.      0.01   1.0E-19   1.0E-19   1.0E-18      2.30      920.

    3           .40       .05        1.        1.
    7       0.44380   8.01E-2 5.792e-07      5.E7        1.
SHAL2    3     2600.      0.05  24.0E-15  24.0E-15  24.0E-15      3.50      920.

    3           .30       .01        1.        1.
    7       0.44380   8.01E-2 5.792e-07      5.E5        1.
DEEP3    3     2600.      0.03   5.0E-15   5.0E-15   5.0E-15      3.50      920.

    3           .40       .05        1.        1.
    7       0.44380   8.01E-2 5.792e-07      5.E6        1.
ATMO4    3     2600.      0.99   1.0E-19   1.0E-19   1.0E-18      2.30    99920.

    3           .40       .05        1.        1.
    7       0.44380   8.01E-2 5.792e-07      1.E5        1.

SELEC----2----3----4----5----6----7----8----9---10---11---12---13---14---15---16
    1              1                            0    1             0    3    2
       3.

MULTI----1----*----2----*----3----*----4----*----5----*----6----*----7----*----8
    3    4    3    6
START
PARAM----1----*-123456789012345678901234----*----5----*----6----*----7----*----8
 8 49999     1001000301 0020 00300  3
        .0  8.64E+11       -1.                       9.8065
     1.E-9       1.0
     1.E-5        1.                                  1.e-8              1.e+4
                235.0              .0030            0.000001              3.0E5
|
ELEME
A11 1          ATMO4 .1000E+52 .1000E+05          0.5000E+020.5000E+020.5000E+03
A21 1          CAPR1 .1000E+070.0000E+00          0.5000E+020.5000E+020.4500E+03
A31 1              1 .1000E+070.0000E+00          0.5000E+020.5000E+020.3500E+03
```

**Figure 1:** Example of TOUGH2 input file.

Here I supply a brief description of the main keywords. For a detailed description of the format and for a complete description on how to write the TOUGH2 input file, the reader is referred to the TOUGH2 v.2.0 manual [Pruess et al., 1999]. The keyword ROCKS describes the rock types providing

the hydrogeologic parameters (porosity, permeability, heat conductivity, specific heat, etc.). The keywords ELEME and CONNE provide the geometric information about the mesh (nodes coordinates, interfaces areas, etc), and in ELEME it is also specified the rock type for each grid block. The keyword MULTI is used in order to specify the number of fluid components and balance equations per grid block. SELEC is used to provide thermophysical property data. PARAM is the keyword dedicated to define the computational parameters, such as time stepping, simulated time and program options. Using the keyword GENER it is possible to define the sinks and sources. With the keywords INCON and INDOM it is possible to specified the initial condition.

### 2.1.4 EWASG EOS MODULE

EWASG (Equation-of-state for Water, Salt and Gas) is a EOS module for TOUGH2 V.2.0 used primarily for modeling hydrothermal systems containing dissolved solids and one non-condensable gas (NCG) such as $CO_2$, $CH_4$, $H_2S$, $N_2$ and $H_2$ [Battistelli et al., 1997]. Such components are typical of geothermal reservoir. The limits of validity of thermodynamic correlations implemented in EWASG are up to 350°C and up to 1000 bar for $H_2O$-NaCl-NCG mixtures [Battistelli et al., 2012], with the limitation of low to moderate NCG partial pressures. In literature, it is possible to find several applications of the EOS EWASG. Battistelli and Nagy (2000) used it to evaluate the exploitation of geothermal resources in Skierniewice area in Poland characterized by high salinity aquifer at a temperature equal to 70°C. Battistelli et al. (2002) tested a conceptual model of Dubti geothermal field (Ethiopia) by using a simple 3D model. Crestaz et al. (2002) applied EWASG for the modeling of sea water intrusion in coastal plains of the Dominican Republic. Weisbrod et al. (2005) modeled the salt accumulation and precipitation due to water evaporation from soil fractures. Battistelli and Marcolini (2012) used EWASG supported by the pre- and post-processor

Petrasim to model the natural state and simulate the production forecast for Lumut Balai geothermal field, Indonesia. Battistelli (2013) used EWASG supported by Petrasim to model the natural state and simulate the production forecast for Patuha geothermal field, Indonesia. Sirait et al. (2015) used EWASG supported by Petrasim to model the natural state and simulate the production forecast for the Dieng field, Indonesia. Other researchs are related to the investigation of the use of TOUGH2-EWASG for the modelling of halite formation in natural gas storage aquifers [Lorenz and Muller, 2003] and for the numerical simulation of salt water injection into a depleted geothermal reservoir [Calore and Battistelli, 2003; Geloni and Battistelli, 2010]. Flint and Ellett (2003) employed EWASG to model the artificial recharge of an aquifer in California, USA. Pruess et al. (2002) applied EWASG to study the hydrogeological processes developing outside the buried tanks and containing high level nuclear wastes at Hanford site, USA. Esposito and Augustine (2014) used EWASG to model the exploitation of a geopressured resource located in Texas, USA. Purwanto and Kaya (2015) modeled geothermal reservoirs in Waiotapu-Waikite-Reporoa areas, New Zealand. Blanco Martìn et al. (2015) applied EWASG with the TOUGH-FLAC simulator to model the coupled hydrodynamic and geomechanical processes in a generic salt repository for heat-generating nuclear wastes. Ratouis et al. (2016) performed simulations of the Rotorua geothermal field (New Zealand).

### 2.1.4.1 Thermodynamic description

A detailed description of the thermodynamic capability of EWASG is proposed by Battistelli et al. in a paper published in 1997 [Battistelli et al., 1997]. Here the aim is to outline the main features, the improvements

dedicated to update EWASG in the last years [Battistelli, 2012] and the characteristic correlations.

As stated before, EWASG describes a system composed by tree phases (solid, liquid and gas) and neglecting the case of single solid phase, the remaining combination are six. Table 1, created starting from Battistelli et al., 1997, lists the primary variables for each thermodynamic state. The code is able to determine the passage from a thermodynamic state to another by controlling the main thermodynamic variables of the system. For example, in the case of liquid conditions, the code checks the value of the pressure comparing it with the boiling pressure curve. Solid salt phase pops up if the salt mass fraction in the liquid phase exceeds the solubility of solid salt. In gas conditions it is possible for liquid to appear only if its partial pressure is greater than the vapour saturated brine pressure.

**Table 1:** Primary variable sets in EWASG [Battistelli et al., 1997]

| **Thermodynamic condition** | **Primary variables** | | | |
|---|---|---|---|---|
| | **1** | **2** | **3** | **4** |
| Liquid | Total pressure (liquid) | Salt mass fraction (liquid) | NCG mass fraction (liquid) | Temperature |
| Gas | Total pressure (gas) | Salt mass fraction (gas) | NCG mass fraction (gas) | Temperature |
| Liquid + gas | Total pressure (gas) | Salt mass fraction (liquid) | Gas phase saturation | Temperature |
| Liquid + solid | Total pressure (liquid) | Solid saturation | NCG mass fraction (liquid) | Temperature |
| Gas + solid | Total pressure (gas) | Solid saturation | NCG mass fraction (gas) | Temperature |
| Liquid + gas + solid | Total pressure (gas) | Solid saturation | Gas phase saturation | Temperature |

Finally, in the case of liquid-gas mixture the code examines the gas phase saturation ($S_G$): in a two-phase fluid system, when $S_G$ becomes equal or exceeds the value $1\text{-}S_S$ (= $S_G+S_L$) then the gas phase appears replacing the

liquid phase. If the gas saturation assumes a negative value then the gas phase disappears and the single-liquid phase takes place. In the original version of EWASG pure water properties were computed using the International Formulation Committee correlations [IFC, 1967], but in the latest version these properties are computed using the IAPWS-IF97 correlations [Battistelli, 2012]. Different correlations for computing saturation pressure, density and internal energy for liquid water and steam are defined according to the different regions of the phase diagram (shown in Figure 2): liquid, vapour, super-critical and two-phase.

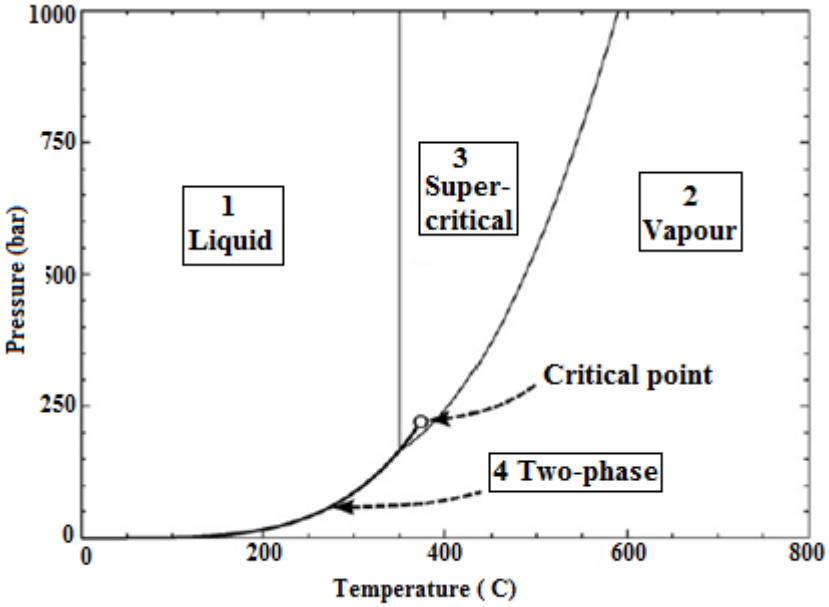


**Figure 2:** Phase-pressure diagram for the IAPWS-97 [Croucher and O'Sullivan, 2008].

In region 1 the thermodynamic conditions are those of the liquid phase, up to 350°C and 1000 bar. Region 2 describes the thermodynamic condition of steam up to 800°C and 1000 bar. Region 4 describes the two-phase condition up to the critical point (T = 373,946 °C, P = 220,64 bar). Finally, region3, which describes the supercritical condition is not taken into account in EWASG. The correlations for the dynamic viscosity of water and steam are taken from the IAPWS 2008, which provide more accurate viscosity values at high temperature [Battistelli, 2012].

In the latest version of EWASG, some correlations dedicated to the water-salt mixtures, like brine density, brine enthalpy and halite density, are computed using Driesner (2007). For brine density and enthalpy, Driesner proposes correlations between the water-salt solution and a reference substance, i.e. pure water. Starting from the temperature and salt mass fraction of the brine it is possible to compute the temperature $T_V^*$ at which the pure water has the same molar volume. Then the pure water density is determined by IAPWS-97 correlation. Finally, the brine density is computed with the following expression [Battistelli, 2012]:

$$\rho_{brine}\left(T,P,X_{NaCl}\right)=\rho_{H_2O}\left(T_V^*,P\right)\frac{PM_{brine}}{PM_{H_2O}} \tag{2.12}$$

Where $PM_{H_2O}$ is the molecular weight of pure water and $PM_{brine}$ is the brine molecular weight, computed from the salt mass fraction and $\rho_{H_2O}$ is the pure water density. Driesner proposes a similar approach for the determination of brine enthalpy: by computing the temperature $T_H^*$ (function of pressure and salinity) at which the pure water has the same enthalpy of the brine [Driesner, 2007]:

$$h_{brine}\left(T,P,X_{NaCl}\right)=h_{H_2O}\left(T_H^*,P\right) \tag{2.13}$$

A linear relation with the pressure provides the halite density:

$$\rho_{halite}=\rho_{halite}^0+lP \tag{2.14}$$

Where $\rho_{halite}^0$, the halite density at zero pressure and it is temperature dependent. $l$ is a temperature dependent parameter. The correlations cover a range of temperature up to 350°C, with a minor error up to 370°C, the pressure can become up to 1000 bar and the NaCl concentration up to saturation. These correlations are coded into the DRIESNER subroutine.

The halite solubility is computed as a function of temperature, *T*, using a correlation by Potter and quoted by Chou (1987):

$$\alpha=\frac{26.218+0.0072T+0.000106T^2}{100} \tag{2.15}$$

This expression is valid for temperature between 0°C and 800°C and it is coded into HALITE subroutine. Previously the enthalpy of halite was computed by integrating the specific heat provided by Silvester and Pitzer (1976), in the latest version of EWASG, the halite enthalpy is computed using the correlation for the specific heat given by Driesner (2007) in which it is function of both pressure and temperature:

$$c_{P,halite} = b_0 + 2b_1\left(T - T_{triple,NaCl}\right) + 3b_2\left(T - T_{triple,NaCl}\right)^2 + b_3 P + b_4 P^2 \qquad (2.16)$$

where $b_0$, $b_1$ and $b_2$ are known constants, $b_3$ and $b_4$ are obtained solving polynomials with respect the temperature. The integration of eq. (2.16) is made considering the halite enthalpy at triple point of halite as reference state (0 J/kg for enthalpy of pure liquid water at the triple point).

The brine vapour pressure is computed using a correlation by Haas (1976), coded into subroutine SATB. It is based upon the observation of Othmer et al., 1968a and 1968b, that the temperature of the brine ($T_x$) and the temperature of the pure water ($T_0$) at the same pressure are related by the following expression:

$$T_0 = e^{\frac{\ln T_x}{D + D_1 T_x}} \qquad (2.17)$$

Where $D$ and $D_1$ are salt concentration polynomials. By computing the equivalent temperature for pure water, it is then possible to determine the saturation pressure using the pure water subroutine (SAT).

In regard to carbon dioxide component, density and enthalpy are computed using equation from Sutton and McNabb (1977). In particular, for the specific enthalpy they proposed the following expression:

$$h_{CO_2} = 1.667\ 10^6 + 1542T - 794800\log_{10} T + \\ -\frac{4.135\ 10^7}{T} - \frac{0.3571P\left(1 + 7.576\ 10^{-8} P\right)}{\left(T/100\right)^{10/3}} \qquad (2.18)$$

Where $T$ is the temperature (in Kelvin), $P$ is the pressure (in Pascal).

The dynamic viscosity of carbon dioxide is calculated using the correlation by Pritchett et al (1981):

$$\mu = \left( E_0(\mathrm{P}) + E_1(\mathrm{P})\,\mathrm{T} + E_2(\mathrm{P})\,\mathrm{T}^{\,2} + E_3(\mathrm{P})\,\mathrm{T}^{\,3} + E_4(\mathrm{P})\,\mathrm{T}^{\,4} \right) 10^{-8} \qquad (2.19)$$

Where $E_0$, $E_1$, $E_2$, $E_3$ and $E_4$ are pressure dependent coefficients and $T$ is the temperature (in Celsius). This correlation is coded into VISGAS subroutine.

## 2.2 T2Well

As mentioned in the introduction section, T2Well is an extension of TOUGH2, which provides additional capabilities to calculate the flow in wellbore and reservoir. By introducing a special wellbore sub-domain into the numerical grid, denoted by “w” or “x” as initial letter, the code is able to compute the wellbore flow using the Drift Flux Model (DFM) [Zuber and Findlay, 1965]. In the next subparagraph, following the T2Well Manual by Pan et al. 2011, it is reported a survey of the fundamental equation solved by T2Well, a summary of the DFM, a brief description of both the discretized equations and of the analytical heat exchange.

### 2.2.1 Mass and energy balance

The equation for the mass and energy conservation have the same structure as in TOUGH2, eq.2.1:

$$\frac{d}{dt}\int_{V_n} M^k dV_n = \int_{\Gamma_n} \overrightarrow{F^k} \cdot n \; d\Gamma_n + \int_{V_n} q^k dV_n \qquad (2.20)$$

The main difference from the equations used by TOUGH2 for the porous media are in the energy flux, energy accumulation and in the computation of phase velocity. Since the DFM implemented in T2Well is related to the

motion of two phases, the mass accumulation term for the wellbore cells can be written as [Pan et al. 2011]:

$$M^k = \sum_\beta S_\beta \rho_\beta X_\beta^k = S_G \rho_G X_G^k + S_L \rho_L X_L^k \qquad k = 1 \text{ and } 2 \tag{2.21}$$

Where $X_\beta^k$ denotes the mass fraction of the k component in the phase $\beta$, $\rho_\beta$ is the density of the phase $\beta$ and $S_\beta$ stands for the local saturation of the phase $\beta$. The local saturation is computed for both the phases with the sequent relation:

$$S_G = \frac{A_G}{A} = \frac{A_G}{A_G + A_L} \tag{2.22}$$

Where $A$ is the cross-sectional area and $A_G$ and $A_L$ are respectively the cross-sectional area occupied by the gas and the liquid phase over the cross section at a given elevation.

The energy accumulation term for wellbore cells is given by:

$$M^{KN+1} = M^3 = \sum_\beta \rho_\beta S_\beta \left( u_\beta + \frac{1}{2} v_\beta^2 \right) \tag{2.23}$$

Where $u_\beta$ is the internal energy, $\frac{1}{2} v_\beta^2$ is the kinetic energy, both are per unit mass, of the phase $\beta$.

For what concern the flow term, the relation to compute the total advective mass transport for the component k in one dimension is:

$$F^k = -\frac{1}{A} \left( \frac{\partial (\mathrm{A}\, \rho_G\, \mathrm{X}_G^k \mathrm{S}_G\, v_G)}{\partial z} + \frac{\partial (\mathrm{A}\, \rho_L\, \mathrm{X}_L^k \mathrm{S}_L\, v_L)}{\partial z} \right) \tag{2.24}$$

Where z is the coordinate along the wellbore.

The energy flux includes contributes due to advection, kinetic energy, potential energy and lateral wellbore heat loss/gain, and in one dimension can be written as:

$$F^{KN+1} = F^3 = -\lambda \frac{\partial T}{\partial z} - \frac{1}{A} \sum_\beta \frac{\partial}{\partial z} \left( A \rho_\beta S_\beta v_\beta \left( h_\beta + \frac{v_\beta^2}{2} \right) \right) - \sum_\beta \left( S_\beta \rho_\beta v_\beta g \cos\theta \right) - Q_{ex} \tag{2.25}$$

Here $h_\beta$ denotes the specific enthalpy of the fluid phase $\beta$, $g$ is the module of gravitational acceleration and $Q_{ex}$ is the terms that take into account for the heat loss or gain of wellbore per unit length of wellbore (optional if the surrounding formation is not represented in the numerical model). $\theta$ is the angle between wellbore section and vertical direction. $T$ is the temperature and $\lambda$ is the area-averaged thermal conductivity of the wellbore.
The velocity of both phases, gas and liquid, are computed using the DFM, which is described in the next paragraph.

## 2.2.2 Drift Flux Model

First developed by Zuber and Findlay (1965), the Drift Flux Model represent a valid alternative for the study of two-phase flow in a pipe, in particular for the determination of the phase velocities, without solving the momentum equation for each phase.
The Drift Flux Model is based on the empirical constitutive relationship (all variables in the following development have to be considered as area-averaged or assumed to be constant over a cross-section):

$$v_G = C_0 j + v_d \tag{2.26}$$

Which stands that the gas velocity $v_G$, can be related to the volumetric flux of the mixture $j$, and the drift velocity of the gas, $v_d$, via the parameter $C_0$, named profile parameter, which takes in account for the effect of local gas saturation and velocity profiles over the pipe cross-section [Pan et al, 2011].
By definition, the volumetric flux of the mixture is:

$$j = S_G v_G + (1 - S_G)\, \mathrm{v}_L \tag{2.27}$$

Where $v_L$ is the liquid velocity and, combining the equations 2.26 and 2.27, it can be determined as:

$$v_L = \frac{1 - S_G C_0}{1 - S_G} j - \frac{S_G}{1 - S_G} v_d \tag{2.28}$$

The momentum balance in differential form takes the following expression:

$$\frac{\partial \rho \vec{v}}{\partial t} + \nabla \cdot (\rho \vec{v} \vec{v}) = -\nabla p + \nabla \cdot \vec{\tau} + \rho \vec{g} \tag{2.29}$$

Where in the right side there is the time derivative of the momentum rewritten using the Reynolds theorem of transport and in the left side there is sum of the forces: the contact force (pressure and viscous forces) and the gravitational force.

Starting from the equation (2.29) and considering the fluid moving only in the vertical direction (so $v_{\beta x} = 0,\ v_{\beta y} = 0,\ v_{\beta z} = v_\beta$ ), it is possible to reformulate the momentum balance for each fluid phase and then for the entire duct flow [Brennen, 2005]:

$$\frac{\partial}{\partial t}(\sum_\beta \rho_\beta S_\beta v_\beta) + \frac{1}{A}\frac{\partial}{\partial z}(A \sum_\beta \rho_\beta S_\beta v_\beta^2) = -\frac{\partial p}{\partial z} + \frac{\Gamma \tau_w}{A} + \rho_m g \cos\theta \tag{2.30}$$

Where $\rho_\beta$ is the density, $S_\beta$ is the saturation and $v_\beta$ the velocity of the $\beta$ phase, $\tau_w$ is the shear stress, $A$ is the cross-sectional area of the well, $\Gamma$ is the perimeter of the cross-section, $\theta$ is the local angle between wellbore section and the vertical direction and $\rho_m$ is the mixture velocity, defined as:

$$\rho_m = \sum_\beta S_\beta \rho_\beta \tag{2.31}$$

Now consider a fluid composed by only two phase: liquid and gas.

Considering the mixture in its entirety, the relation of Darcy-Weisbach assumed that the stress is proportional to the square of the mixture velocity:

$$\tau_w = \frac{1}{2} f \rho_m |v_m| v_m \tag{2.32}$$

In which compares the Fanning friction factor, $f$ , which is a function of the Reynolds number (Re), and it is defined as follows:

$$\begin{aligned} f &= \frac{16}{\mathrm{Re}} && \textit{for} \quad \mathrm{Re} < 2400 \\ \frac{1}{\sqrt{f}} &= -4\log\left[\frac{2\varepsilon/\mathrm{d}}{3.7} - \frac{5.02}{\mathrm{Re}}\log\left(\frac{2\varepsilon/\mathrm{d}}{3.7} + \frac{13}{\mathrm{Re}}\right)\right] && \textit{for} \quad \mathrm{Re} > 2400 \end{aligned} \tag{2.33}$$

Where $\varepsilon$ is the wellbore roughness, $d$ is the wellbore diameter and the Reynolds number is defined as:

$$\mathrm{Re} = \frac{\rho_m u_m d}{\mu_m} \tag{2.34}$$

Introducing the following quantity, the mixture density:

$$\rho_m = S_G\rho_G + (1 - S_G)\rho_L \tag{2.35}$$

andthe mixture velocity

$$v_m = \frac{S_G\rho_G v_G + (1 - S_G)\rho_L v_L}{\rho_m} \tag{2.36}$$

Pan et al. obtained the momentum equation in terms of the mixture velocity [Pan et al., 2001, T2well manual, appendix A]:

$$\frac{\partial}{\partial t}(\rho_m v_m) + \frac{1}{A}\frac{\partial}{\partial z}\left[A\left(\rho_m v_m^2 + \varsigma\right)\right] = -\frac{\partial p}{\partial z} - \frac{\Gamma f \rho_m |v_m| v_m}{2A} - \rho_m g\cos\theta \tag{2.37}$$

Where $\varsigma$ is a term that takes in account of the slip between the two phases and is equal to:

$$\varsigma = \frac{S_G}{1 - S_G}\frac{\rho_G\rho_L\rho_m}{\rho_m^{*2}}\left[\left(C_0 - 1\right)u_m + u_d\right]^2 \tag{2.38}$$

And $\rho_m^*$ is the profile-adjusted average density:

$$\rho_m^* = S_G C_0\rho_G + (1 - S_G C_0)\rho_L \tag{2.39}$$

The DFM permits to determine the velocities of the phases of two-phase flow by computing the mixture velocity with the equation (2.37), a simplified momentum equation, and by determining the drift velocity from some empirical relationships [Shi et al., 2005]. The phase velocities then are computed with the following equations:

$$
\begin{aligned}
v_G &= C_0 \frac{\rho_m}{\rho_m^*} v_m + \frac{\rho_L}{\rho_m^*} v_d \\
v_L &= \frac{\left(1 - S_G C_0\right)\rho_m}{\left(1 - S_G\right)\rho_m^*} v_m - \frac{S_G \rho_G}{\left(1 - S_G\right)\rho_m^*} v_d
\end{aligned}
\tag{2.40}
$$

The remaining task is to estimate both the drift velocity and the profile parameter. Shi et al. (2005) introduced the functional forms for the determination of the drift velocity and the profile parameter implemented in T2Well (See T2Well manual for further details).

## 2.2.3 Discretized equations

The approach used by Pan et al., 2011, to solve the momentum equation (eq. 2.37) is based on a hybrid formulation at the interfaces of neighboring wellbore cells obtained solving semi-explicitly:

$$
v_m^{\kappa+1} = \frac{\left(\frac{\partial P}{\partial z} - \rho_m g \cos\theta\right)^{\kappa+1} + \frac{1}{\Delta t}\rho_m^{\kappa} v_m^{\kappa} - \left[\frac{1}{A}\frac{\partial}{\partial z}\left(A\sum_{\beta}\rho_{\beta} S_{\beta} v_{\beta}^2\right)\right]^{\kappa}}{\frac{\rho_m^{\kappa+1}}{\Delta t} + \frac{f^{\kappa}\Gamma\rho_m^{\kappa+1}\left|v_m^{\kappa}\right|}{2A}}
\tag{2.41}
$$

Where $\kappa$ and $\kappa+1$ indicate the previous and the current time step. For what concern the mass and energy conservation equations of eq. (2.20), they are discretized using a backward, first-order, fully implicit finite difference scheme:

$$
\begin{aligned}
&\left[M_i^{k,\kappa+1} - M_i^{k,\kappa}\right]\frac{V_i}{\Delta t} = F_{i,i+\frac{1}{2}}^{k,\kappa+1} - F_{i,i-\frac{1}{2}}^{k,\kappa+1} + Q_i^{k,\kappa+1} \\
&k = 1, 2 \ \textit{and}\ 3
\end{aligned}
\tag{2.42}
$$

## 2.2.4 Heat exchange

The heat exchange between the wellbore and the formation can be computed in two ways: If the surrounding formation is explicitly defined in the

numerical grid, then the heat exchange computation takes place as the normal heat flow term of TOUGH2. Otherwise, by imposing a negative value at the heat conductivity in the ROCKS type domain of the wellbore, the heat exchange is computed analytically. In the last case the heat loss/gain contribution of eq. (2.25) for the i[th] wellbore cell takes the form:

$$Q_{ex,i} = -A_{wi}\lambda_{wi}\left(\frac{T_i - T_\infty(z)}{rf(t)}\right) \tag{2.43}$$

Where $A_{wi}$ is the contact area between wellbore and formation of the i[th] wellbore cell, $\lambda_{wi}$ is the thermal conductivity of the formation surrounding the i[th] wellbore cell, $T_i$ is the temperature of the i[th] well grid block, $T_\infty(z)$ the temperature of the formation, *r* the radius of the wellbore and *f(t)* is the Ramey's heat loss function [Ramey, 1962] as proposed by Kanev et al. (1997):

$$f(t) = \frac{1}{-\ln\left(\frac{r}{2\sqrt{\alpha t}}\right) - 0.29} \tag{2.44}$$

α is the thermal dispersivity of the surrounding formation.

## 2.3 VORO2MESH and TOUGH2Viewer

As stated in the Background chapter, in the last few years the geothermal research group of DICAM has focused his efforts in order to better manage the information required to realize the TOUGH2 input files and to browse its output files. For this goal, in particular, the research group has realized TOUGH2Viewer, a 3D visualization and post-processing tool, and VORO2MESHa software coded in C++, based on the voro++ library, dedicated to create fully Voronoi 3D grid. Geological shape surfaces reconstruction is a very important feature useful in many scenarios, e.g. in

case of double phase migration process, due of structural traps (highs), or when it is necessary a local refinement. Structured grids are simple to create and to manage, but they are unable to follow the surface profile of geological body, or to realize local refinement, without substantially increase the number of grid blocks. 3D Voronoi grids, which are IFDM compliant - because there is orthogonality between the segment connecting the nodes and the interface area between blocks - offer a great degree of flexibility. The Voronoi grids are an example of Voronoi diagrams application. In this chapter, it is presented a brief summary of grid type, as defined by Berry et al., 2014, then it follows the description of Voronoi diagrams and of the software VORO2MESH and TOUGH2Viewer.

### 2.3.1 Grid type

The spatial domain discretization can be performed using structured or unstructured grids. Structured grids allow to implicitly define the position of all the grid nodes and the connections along x and y axes. Structured grids can be regular if all the blocks have the same size and shape, or irregular when the spacing between the blocks varies (along one or more coordinates). Unstructured grids require that the position of the grid nodes and their connections are explicitly defined, furnishing coordinates and geometrical information for each of them. For modelling purpose could be necessary to refine the grid. This can be done either on structured and unstructured grids. It is possible to distinguish between the global refinement and the local refinement. In the former all the grid blocks are interested by the refinement process, and can be realized using either a structured regular grid or an unstructured grid; the second allows to increment grid resolution only in a region of interest, and it is obtained either generating a structured irregular (telescopic) grid (Townley and Wilson, 1980) or a Voronoi grid.

## 2.3.2 Voronoi diagrams

First introduced by Voronoi in 1908, they play a remarkable role not only in mathematical and applied natural science, but also in the application of various algorithms in computer science [Aurenhamer, 1991]. Aurenhamer provides a general definition of Voronoi diagrams and in the following it is briefly described. Being Z a set of *n* points (called *sites* by Aurenhamer, we refer to them as *nodes*) in the plane. Considering two distinct nodes *p* and *q*, such as $p, q \in Z$, the *dominance* of *p* over *q* is defined as the subset of the plane being at least as close to *p* as to *q*:

$$dom(p,q) = \left\{ x \in \mathbb{R}^2 \mid \delta(x,p) \leq \delta(x,q) \right\} \tag{2.45}$$

Where $\delta$ denotes the Euclidean distance. It is called *separator* the perpendicular bisector of *p* and *q* and it divides the plane in two regions: the one in which all points are closer to *p* and the one in which all points are closer to *q*. Finally, the *region* of a node $p \in Z$, is defined as intersection of all the *dominances* of *p*:

$$reg(p) = \bigcap_{q \in S - \{p\}} dom(p,q) \tag{2.46}$$

Partitioning in this way a plane in which are present *n* nodes, results in the presence of at least *(n-1)edges*, an edge is the straight segment which separates two *dominances*, and *vertices* (the endpoints of edges). As a result from the definition of *dominance* it follows that each point on an *edge* is equidistant from two *nodes* and that each *vertices* is equidistant from at least three *nodes* (since it belongs to at least three *dominance*). This partition of the plane is called *Voronoi diagrams, V(Z),* of the finite point set *S*. The definition of *Voronoi diagrams* can be extended to three dimension: being *Z* a set of *nodes* in the 3D space. Considering two distinct nodes *p* and *q*, such as $p, q \in Z$, the *dominance* of *p* over *q* is defined as the subset of the space being at least as close to *p* as to *q*:

$$dom(p,q) = \left\{ x \in \mathbb{R}^3 \mid \delta(x,p) \leq \delta(x,q) \right\} \tag{2.47}$$

In this case the *separator* is represented by a plane whose points are equidistant from *p* and *q*. The *region* of a generic node is defined as eq. 2.46. Partitioning in this way the space in which are present *n* nodes, results in the presence of at least*(n-1) interfaces,* the interface is the portion of plane which separates two *dominances,* and *vertices* (common points of at least three *dominance*). In this way the space can be divided into polyhedrons, to each of which a node is assigned. It follows from the construction of the partition of the space that each line connecting two neighboring nodes is perpendicular to the interface which separates the two *dominance.* Hereafter we refer to the grid obtained with the Voronoi approach as fully 3D Voronoi grid.

### 2.3.3 VORO2MESH

The information required by TOUGH2 as input for the definition of the geometry of the grid are: the coordinates of each grid block, the volume of each grid block, the area of interfaces of each polyhedron, the distance between each node and the interfaces of the polyhedron which contains it and, for each connection (given a node, a connection is established with each neighboring node), the direction of the line connecting two neighboring nodes, defined referring to the gravitational acceleration vector. For the visualization of this kind of grids more information is necessary, such as the coordinates of the vertices of each polyhedron.

VORO2MESH permits to build a space discretization of a convex domain, starting from a set of nodes (called also seed points), applying the Voronoi approach. In a Euclidean space a convex domain is a set of points in which, the segment that connects each couple of point, is entirely contained in the set. Using the voro++ library it is possible to define the vertices coordinates, surface area and volume of each polyhedron block of the grid. Giving as input a set of geological surfaces, VORO2MESH is able to set up the nodes of the

grid. The result is a hybrid grid characterized by orthogonal prisms (regular blocks) in regions far from the surfaces and Voronoi blocks close to the surface contact between different geological formations. This shrewdness allows limiting the average number of connections. For further details, the reader is referred to the TOUGH symposium conference paper of Bonduà et al., 2015.

### 2.3.4 TOUGH2Viewer

TOUGH2Viewer [Bonduá et al., 2012], is a post-processor dedicated to the visualization of TOUGH2 output file (see Figure 3). Some of the applications include: visualization of simulation results, variable profile along with depth, realization of contour plot, etc. It is developed in Java using the Java3D library. Initially designed for the visualization of structured grid and 2D Voronoi grids (regular vertically discretized) the latest version is improved with new functionalities to allow managing fully unstructured grids created with VORO2MESH or by means of the voro++ library [Bonduá et al., 2015].

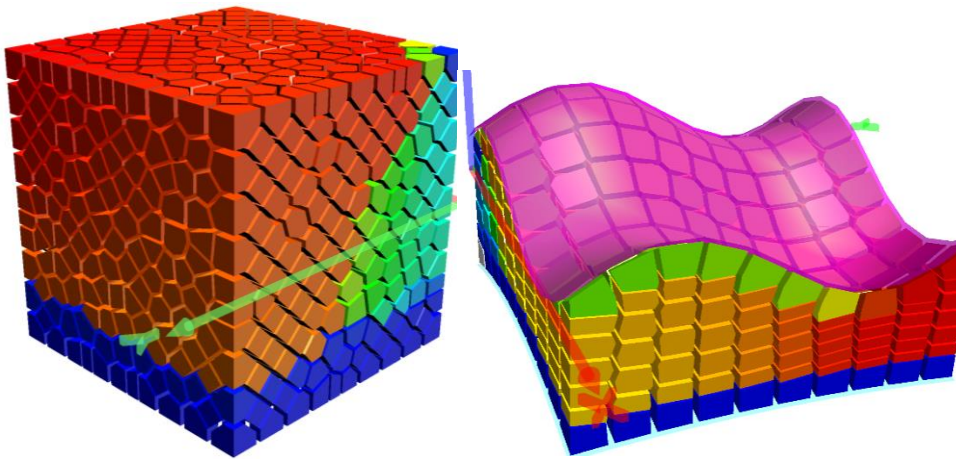

**Figure 3:** Example of model visualization with TOUGH2Viewe

# 3 T2Well-EWASG Development

In this chapter the main modifications of T2Well are described. Besides coupling T2Well with EWASG, some modifications to the analytical computation of heat exchange have been introduced, in order to enhance the capabilities of T2Well.

## 3.1 Analytical computation of heat exchange

The analytical computation of the heat exchange between wellbore and formation allows a considerable simplification of the grid (In fact, in this case, it is necessary to represent only the wellbore), reducing both the efforts to manage the model and the computational time. The methods implemented in the original version of T2Well have some limitations. Since Ramey method provides accurate solutions only for times longer than approximately a week, it is not applicable to reproduce short transient phenomena. The Zhang's method [Zhang et al., 2011] is based on the superposition of the effects but it does not take into account the thermal resistance related to well completion. To overcome these limitations, the analytical function for heat exchange between the wellbore and the formation has been modified by incorporating the Chiu and Thakur function [Chiu and Thakur, 1991]. Furthermore, it has been introduced the possibility to take into account the completion of the wellbore. In the following, the conceptual model introduced by Ramey in 1962 is described. At a generic depth the fluid inside the wellbore (of radius

$r_1$) is at temperature $T_1$. The radius and the temperature of the completion are respectively $r_2$ and $T_2$. For the computation of heat exchange the sequent hypothesis are assumed:

- The thermal properties of formation and of the completion materials do not change with temperature;
- The heat flux inside the formation is radial and leads by conduction;
- Inside the completion heat flux is so rapid that a steady solution can be assumed. In practice, the thermal capacities of the completion materials are neglected.

The heat flux inside the completion of the wellbore can be written as:

$$dq_1 = 2\pi r_1 U \left(T_1 - T_2\right) dZ \tag{3.1}$$

Where $U$ is the over-all heat transfer coefficient ($W°C^{-1}m^{-2}$).
The heat flux inside the formation:

$$dq_2 = 2\pi\lambda \left(T_2 - T_E\right) f(t_D) dZ \tag{3.2}$$

Where:

- $f(t_D)$ is a time function which describes the trend of heat flux;
- $t_D = \frac{at}{r_2^2}$ is the dimensionless time, with $a = \frac{\lambda}{\rho C}$, $C$ is the specific heat and $\rho$ is the density of the formation;
- $\lambda$ is the thermal conductibility of the formation;
- $T_E$ is the formation temperature.

Equating the heat fluxes (3.1) and (3.2) it is possible to find an expression for $T_2$:

$$T_2 = \frac{\lambda T_E f(t_D) + r_1 U T_1}{\left(r_1 U + \lambda f(t_D)\right)} \tag{3.3}$$

Substituting (3.5) in (3.1):

$$dq_1 = \frac{2\pi r_1 U f(t_D)\left(T_1 - T_E\right)}{\left(r_1 U + \lambda f(t_D)\right)} dZ \tag{3.4}$$

The last equation is an expression for the heat flux between wellbore and formation that takes into account of the completion of the wellbore. Eq. (3.2) can be derived from eq. (3.4) by imposing the completion radius equal to the wellbore radius and the over-all heat transfer coefficient equal to infinity.
Willhite (1967) provided the relation for the computation of the overall heat transfer coefficient.
The computation of the over-all heat transfer coefficient U is carried out considering a radial flux through the completion as series of thermal resistors completion. The expression derived by Willhite for U, is:

$$U = \left[ \frac{r_{to}}{r_{ti} h_f} + \frac{r_{to} \ln \frac{r_{to}}{r_{ti}}}{\lambda_{tub.}} + \frac{1}{(y_c + y_r)} + \frac{r_{to} \ln \frac{r_{co}}{r_{ci}}}{\lambda_{cas.}} + \frac{r_{to} \ln \frac{r_h}{r_{co}}}{\lambda_{cem.}} \right]^{-1} \quad (3.5)$$

Where:

| | |
|---|---|
| $r_{ti}$, $r_{to}$ | Inner and outer tubing radius (m); |
| $r_{ci}$, $r_{co}$ | Inner and outer casing radius (m); |
| $r_h$ | Outer cementation radius (m); |
| $y_f$ | Film coefficient for heat transfer or condensation coefficient ($W°C^{-1} m^{-2}$); |
| $y_c$ | Heat transfer coefficient for natural conduction ($W°C^{-1} m^{-2}$); |
| $h_r$ | Heat transfer coefficient for radiation ($W°C^{-1} m^{-2}$). |
| $\lambda_{tub.}$ | Tubing thermal conductivity ($W°C^{-1} m^{-1}$) |
| $\lambda_{cas.}$ | Casing thermal conductivity ($W°C^{-1} m^{-1}$) |
| $\lambda_{cem.}$ | Cement thermal conductivity ($W°C^{-1} m^{-1}$) |

Assuming that the inner tubing wall is in thermal equilibrium with the fluid and that the tubing and casing resistors are negligible, the expression for the over-all heat transfer coefficient becomes:

$$U = \left[ \frac{1}{h_c + h_r} + \frac{r_{to} \ln \frac{r_h}{r_{co}}}{\lambda_{cem.}} \right]^{-1} \tag{3.6}$$

In particular, for geothermal application, in the case of fluid flux directly in the casing the relation for *U* becomes:

$$U = \frac{\lambda_{cem}}{r_1 \ln \frac{r_2}{r_1}} \tag{3.7}$$

Where $r_1$is the wellbore radius and $r_2$ is the completion radius.

Carslaw and Jaeger proposed an exact solution for the function $f(t_D)$ [Carslaw and Jaeger, 1959]. Their solution is referred to the computation of heat flux at the surface of an infinite cylinder at constant temperature. In their approach it is introduced the dimensionless time defined as:

$$t_D = \frac{\alpha t}{r^2} \tag{3.8}$$

where *t* is the time (s), *r* is the wellbore radius (m) and $\alpha$ is the thermal diffusivity and is equal to $\lambda/(C\rho)$, where $\lambda$ is the thermal conductivity ($Wm^{-1}°C^{-1}$), $\rho$ is the density ($kg\ m^{-3}$) and *C* is the specific heat ($J\ kg^{-1}\ C^{-1}$) of the formation.

As described by Zhang et al., 2011, the Carsaw and Jeager function $f(t)$is equal to:

$$f(t_D) = \frac{2}{\ln(4t_D) - 2\gamma} - \frac{\gamma}{\left(\ln(4t_D) - 2\gamma\right)^2} \tag{3.9}$$

With $\gamma$ denoting the Euler constant.

If $t_D > 2.8$, and it is equal to:

$$f(t_D) = \frac{1}{\sqrt{\pi t_D}} + \frac{1}{2} - \frac{1}{4}\sqrt{\frac{t_D}{\pi}} + \frac{1}{8} t_D \tag{3.10}$$

if $t_D \leq 2.8$.

In 1991, Chiu and Thakur proposed an empirical expression for $f(t_D)$:

$$f(t_D) = \left(0.982 \ln\left(1+1.81 t_D\right)\right)^{-1} \tag{3.11}$$

Which is in good agreement with the exact solution for all the times as displayed by Figure 4.

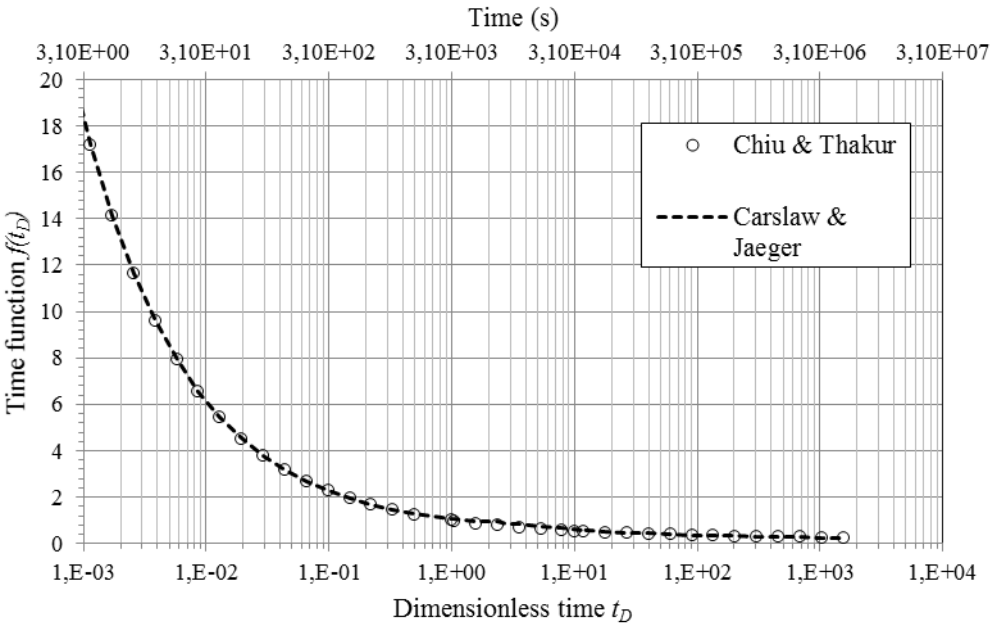


**Figure 4:** comparison between the time functions proposed by Carslaw and Jaeger (dashed line) and Chiu and Thakur (circles).

Since the Chiu and Thakur time function is represented by a single relation, both for early and long times, it is preferable to the Carsaw and Jeager function in order to avoid discontinuities.

## 3.2 T2Well source code

The T2Well source code used in this work is a beta-version and it has been provided by the author Dr. Lehua Pan. In Table 2 a description of the source modules is furnished as described by Pan et al. 2011.

**Table 2** Source code file for T2Well [Pan et al. 2011].

| File name | Description |
|---|---|
| agra.f | Contains a routine to save a time series of flow rates through user-defined horizons and a routine to save liquid and gas volume vs. time to disk file DOFT. |
| DFM_new.f | Welbore flow model definitions, subroutines and functions (Drift Flux Model). |
| mudfv.f | Modified TOUGH2 subroutines CYCIT, MULTI, OUT,..etc, wellbore simulation subroutine CalMixtureVelocity. |
| t2cg22x_well.f | TOUGH2 main program. |
| t2f_well.f | TOUGH2 subroutine. |
| meshm.f | Meshmaker. |
| t2solv.f | Conjugate gradient linear equation solvers. |
| T2 | INCLUDE file with parameters for dimensioning major arrays. |
| EOS.f | Equation of state file. |

Using as EOS source file the file Ewasg.f it is possible to obtain T2Well-EWASG. The code is in FORTRAN 90 and it has been modified, debugged, and compiled using the IDE Visual Studio 2010 Professional. The compiler used was the Intel Composer 2011. The code has been compiled in 32 bit mode.

The next paragraph describes the instruction for the input file set up, highlighting the new input parameters for the modified analytical computation of heat exchange.

## 3.3 T2Well input file

The new relation for the heat exchange computation between wellbore and formation is applied optionally on the basis of the input file. In particular, all the parameters are stored under the keyword ROCKS, and they have to be introduced only for the wellbore ROCKS types, as follows:

```
ROCKS----1----*----2----*----3----*----4----*----5----*----6----*----7----*----8
wellb  NAD    2600.0       1.0   1.0E-13   1.0E-13   1.0E-13      -2.1    1000.0
0.0       0.0       2.1       0.0       0.0
    1            0.2       0.1       0.9       0.7
    1            0.0       0.0       1.0
 NTEMP           RWB       UHT
      ZF(1)    TF(1)
      ZF(2)    TF(2)
…
  ZF(NTEMP)    TF(NTEMP)
```

The first four record are the traditional ones, which refer to the rocks properties (such as density, porosity, permeability, thermal conductibility, specific heat in the first record, pore compressibility and expansivity, heat conductivity in desaturated conditions, tortuosity factor and Klinkenberg parameter in the second record, relative permeability function parameters in the third record and capillary pressure function in the fourth record), to whom the new ones follow. The new record is read by the software only if NAD (second field of the first record) is greater than 3. In this way, after the capillary pressure record, it is possible to introduce the following parameters:
**NTEMP**- number of couples (cell depth; formation temperature) with which the code will determine the corresponding formation temperature at the wellbore cell depth. If NTEMP is equal to 0, then the temperature of the formation is taken equal to the initial wellbore temperature, otherwise the

code will read the couples depth-temperature in the following NTEMP records;

**RWB**- the radius of the completion in meters;

**UHT**- the over-all heat transfer coefficient;

Due to the TOUGH2 settings it is possible, by proper rock type introduction, to take in account different parts for the same wellbore, characterized by different parameters, such as the wellbore and the completion radius, the over-all heat transfer coefficient. Furthermore, characterizing the wellbore, for example, with two different rocks type, it is possible to apply the analytical computation of heat exchange only for a wellbore portion, for which, for modelling purpose, the surrounded formation must not be explicitly modelled. In fact, the analytical computation of heat exchange between wellbore and formation is possible if the model is composed only by the wellbore (no grid blocks of surrounding formation) and it is activated if the thermal conductivity (CWET) of the wellbore rock type is negative. In this case if NAD is less equal than 3, then the relation for the heat flux is eq. (3.2), otherwise, introducing the parameters NTEMP, RWB and UTH, the relation for heat flux is eq. (3.4).

# 4 Model Verification &Validation

In this chapter the principal results of the test of T2Well-EWASG are described. Part of the results has been presented at the TOUGH Symposium, LBNL, California, 28-30 September 2015 [Vasini et al., 2015].

## 4.1 Verification and Validation

Once the user realized a software, or a model, there is a procedure, called Verification and Validation (V&V), which allows to ensure the correctness and reliability of the product [Pace, 2004]. The verification is the first phase of the procedure and tries to answer the question: *did I build the thing right?* In other words, the verification checks if the product (in our case the software T2Well-EWASG) is built satisfying some requirements, specifications and conditions which drive the developer in creating the product and if they are correctly implemented. After the verification it follows the validation: *did I build the right thing?* In this case the procedure serves to control if the product meets the purpose for which it has been created. Since T2Well and the implemented DFM has been widely verified [Pan and Oldenburg, 2013], the verification in this study is dedicated to test the modifications made to T2Well-EWASG, in order to check the results of the analytical equation for

the heat flux with and without the wellbore completion effect. Once obtained the verification it has been possible to proceed with the validation. In our case the validation is provided with three case studies. The first two case studies deal with the reproduction of flowing pressure and temperature profile taken from literature. The third case study involves the application of T2Well-EWASG for the interpretation of production tests performing a full coupled wellbore-reservoir simulation.

## 4.2 Verification of analytical heat exchange

To test the reliability of the analytical computation of heat exchange between the wellbore and the formation the model of example 1 explained by Zhang et al. (2011), has been repeated. The results, in terms of heat flux between the wellbore and the formation, have been compared with the ones obtained by numerical computation.

Consider a portion of a wellbore long 1 m. The wellbore is characterized by a radius equal to 0.05 m and is full of water at constant temperature equal to 100°C. The formation surrounding the wellbore is supposed to be at a fixed initial temperature equal to 20°C and it is characterized by a density equal to 2600 kg $m^{-3}$, a thermal conductivity equal to 2.1 $W°C^{-1}m^{-1}$ and a specific heat equal to $10^3$ $J°C^{-1}kg^{-1}$. In the analytical approach the grid of the model represents only the wellbore (at least two blocks are required by T2Well). On the other hand, in the numerical approach, the grid is radial and it represents the wellbore and the surrounding formation discretized with 185 elements. The radial grid is characterized by very fine discretization near the wellbore and the radius of each block is incremented by 5% moving from the wellbore to the outer radial boundary (at about 400 m from well axis). The initial temperature is maintained constant at the lateral boundary during the simulation by setting infinite volume of the outer blocks. The rock type of the

formation is characterized by a negligible permeability ($10^{-20}$ $m^2$) in order to completely avoid mass flux from the wellbore to the formation. The focus in this test is only on the heat flux. The analytic approach results seem to be in good accord with the numerical ones, as it is highlighted by Figure 5, which shows the values of the heat flux between the wellbore and the formation as function of time.

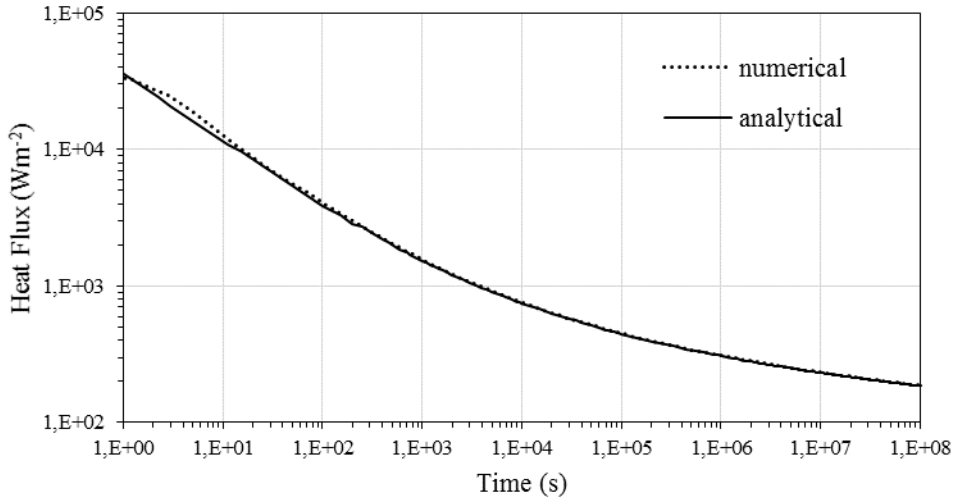


**Figure 5:** Heat flux between the wellbore cell and the formation vs Time, comparison between the numerical and analytical results.

The above simulation has been repeated taking into account the wellbore completion and the analytic approach results have been compared with the results obtained with the numerical approach. In this case the grid for the numerical simulation is composed by the wellbore (r=0.05 m), surrounded by the completion (r=0.10 m), followed by the formations blocks. The radial grid is characterized by very fine discretization near the completion and the radius of the radial grid is incremented by 5% moving from the wellbore completion to the outer radial boundary (at about 450 m from well axis). The initial temperature of the formation is 20°C and it maintained constant at the lateral boundary during the simulation by setting infinite volume of the outer blocks. The thermal conductivity of the completion (cement) has been set at 1.4 $W°C^{-1}m^{-1}$. In order to replicate the assumption made by Ramey (1962) in deriving

eq. (3.4) it has been necessary to set negligible density, porosity and specific heat for the completion. For the simulation using the analytical approach it has been necessary to introduce only two parameters in the input file: the completion radius and the value of the over-all heat transfer coefficient (U= 40.395 $W°C^{-1}m^{-2}$) computed with equation (3.7). A comparison of the heat flux between the wellbore and the formation is displayed in Figure 6.

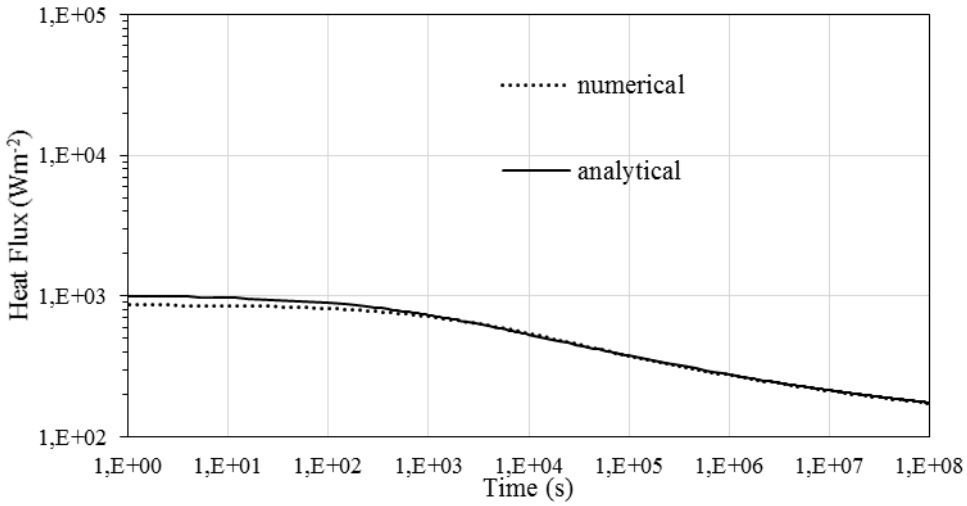


**Figure 6:** Absolute value of the difference between the temperature computed with the numerical approach and the temperature computed with the analytic approach for each time step.

The numerical and analytical results show an agreement in the trend, aside for the times less than about 100 s. Since eq. (3.4) has been derived by Ramey (1962) with the assumption of constant wellbore temperature, it provides unequivocal results when well production, or reinjection, is performed at quite constant conditions as those found for long term production or injection operations. When you want to reproduce short transients driven by rate changes, a more accurate use of eq. (3.4) would need the application of the superposition principle as discussed by Chiu and Thakur (1991) and Zhang et al. (2011). Taking into account that the calculated heat loss is divided by the flowing mass rate in order to assess the effect on fluid enthalpy, when the mass flow in producing geothermal wells is significant, an imprecise

determination of heat transfer vs. time has commonly a negligible effect on fluid enthalpy and flowing temperatures.
In conclusion, the verification allowed to verify the reliability and at the same time to highlight possible weaknesses of the analytical approach. The analytic approach offers a restricted solution which is applicable only when the wellbore is at constant temperature. Since the analytic approach allows to modelling only the wellbore, i.e. simpler grids, it can represent a good compromise. Taking into account of the completion of the wellbore is important, and in this case the analytic approach results to be easier in creating the input file, since the completion is described just with two parameters (the over-all heat transfer coefficient and the completion radius). In the case of numerical approach, it is necessary to represent the completion in the grid design and also to specify a dedicated rock type.

## 4.3 Validation

### 4.3.1 Reproduction of flowing pressure and temperature profiles

In order to validate the T2Well-EWASG's capability to model the wellbore flow in geothermal wells, published data of flowing temperature and pressure logs recorded in geothermal wells have been reproduced. Two short well tests are chosen from literature: the first is about the well W2 [Barelli et al., 1982], the second is about the well KD13 [James, 1975].
For both wells W2 and KD13, the initial wellbore pressure and temperature data was not available. To overcome the lack of information proper initial conditions have been chosen so as to replicate the measured logs assumed to be recorded at closely steady-state wellbore flow. The simulations are designed in order to mimic the well opening and the consequent flow, until

the accomplishment of steady-state conditions, then the flow rate is gradually incremented until the reaching of the target flow rate indicated in literature. The simulation of the well-tests is implemented by setting a GENER sink at the wellhead element in order to extract the fluid at given rate and by specifying constant pressure, temperature and fluid composition at the bottom-hole.

The well W2 is deep 1355 m and produces geothermal fluids characterized by low salinity (9600 ppm) and large amounts of $CO_2$ (2-10%). The wellbore diameter is equal to 13 + 3/8 in. (≈33.9 cm). The bottom hole temperature and pressure, in flowing condition, are 225°C and 98 bar respectively. The initial pressure profile decrease linearly from the bottom pressure set at 98 bar to 400 m, then becomes constant from 400 m to the wellhead. The initial temperature profile is linear, staring from the bottom at 225°C and reaching 35°C at the wellhead. In Figure 7 the profiles of temperature and pressure used as initial conditions are shown.

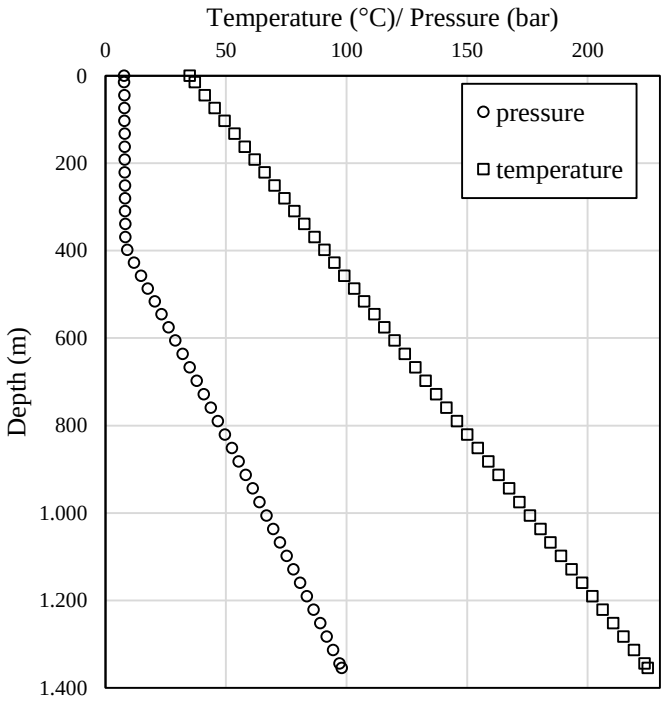


**Figure 7** Profile of pressure and temperature used as initial conditions for the simulation of well W2.

The mesh used has 47 elements, representing only the wellbore, with constant boundary conditions set at the bottom. The initial concentration for $CO_2$ is equal to 30000 ppm and for NaCl is equal to 9600 ppm.

The heat exchange between wellbore and formation is simulated with the analytical approach.

The wellbore KD13 is deep 700 m with a diameter equal to 9 5/8" (0.222 m). The geothermal fluid is characterized by significant concentration of $CO_2$ (20000 ppm) and by low salinity concentration (1000 ppm). The bottom hole flowing temperature and pressure are 193°C and 55.24 bar, respectively. A initial linear temperature profile is set, starting from the bottom at a temperature equal to 200°C and reaching the wellhead at a temperature equal to 100°C. The initial pressure profile is hydrostatic starting from the bottom and at 150 m of depth it becomes constant. In Figure 8 the initial temperature and pressure profiles are shown.

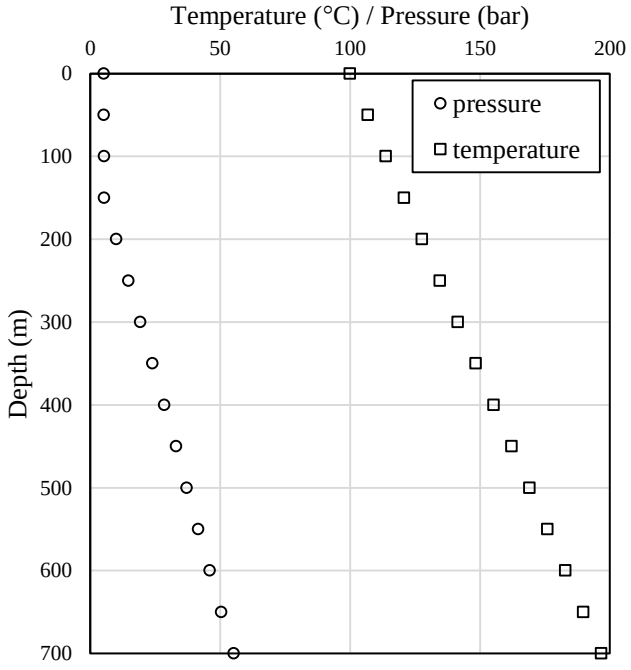


**Figure 8:** Initial condition for pressure and temperature for the production simulation of wellbore KD13.

The mesh is characterized by 15 elements representing only the wellbore, with constant boundary conditions set at the bottom, and the heat exchange is

simulated with the analytical approach. Figure 9 and 10 show the simulated flowing T-P profiles after 11 hours of production at 34.1 kg/s of the wellbore W2. As shown in the Figures 9 and 10, the comparison between the simulated results and the field data is fairly good. The percentage difference between the simulated and experimental temperature values is equal to 0.61% and for the pressure is equal to 2.8%.

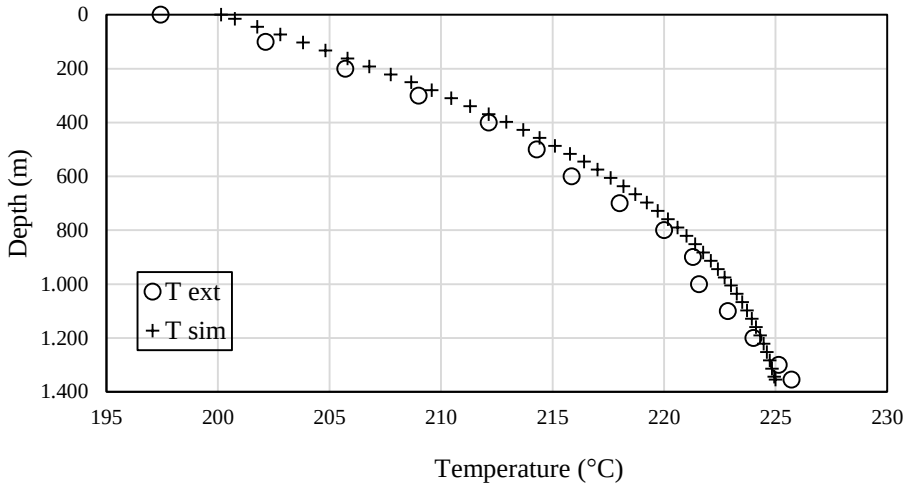


**Figure 9:** Comparison between experimental data and simulation results for the flowing temperature profile of wellbore W2 after 11 hours of production.

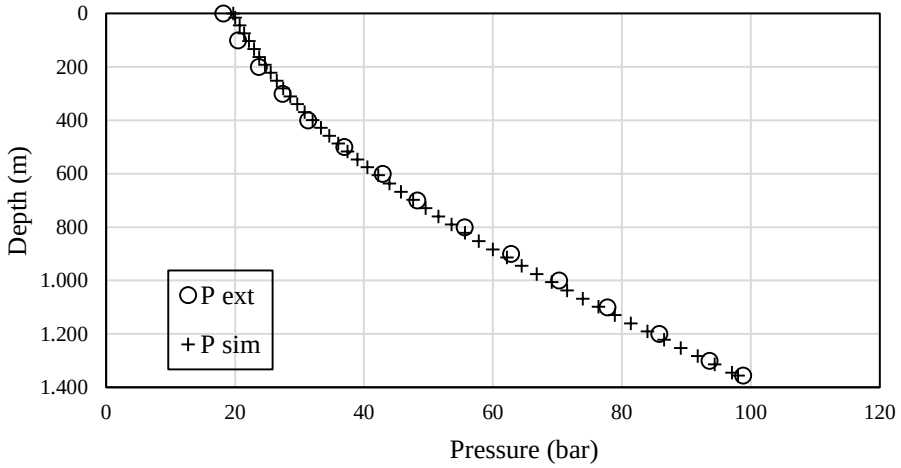


**Figure 10:** Comparison between experimental data and simulation results for the flowing pressure profile of wellbore W2 after 11 hours of production.

Figure 11 displays the flowing temperature profile and figure 12 shows the flowing pressure profile of wellbore KD13, after 100 hours of production test,

with a production rate equal to 90.556 kg/s. Also in this case there is an accordance between the simulated results and the experimental data. The percentage difference for the temperature values is equal to 0.17% and for the pressure values is 0.91%. With this results it is possible to state that T2Well-EWASG is adequate to simulate the wellbore flow in high enthalpy geothermal conditions.

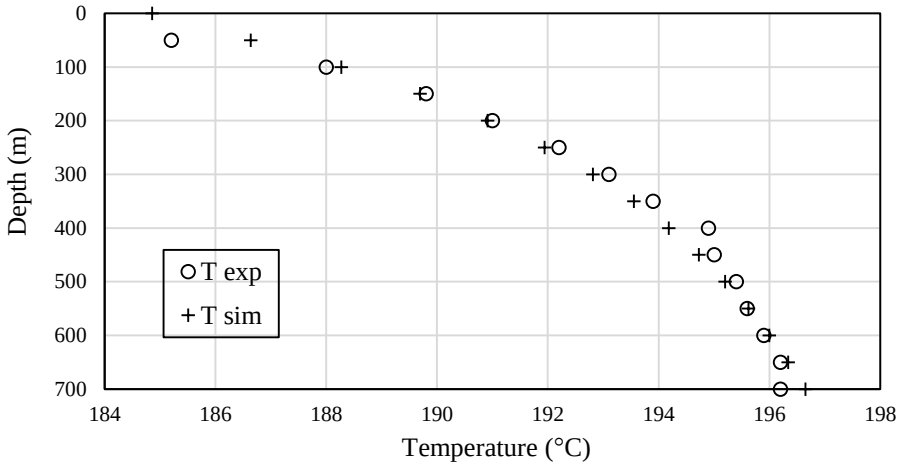


**Figure 11:** Comparison between experimental data and simulation results for the flowing temperature profile of the wellbore KD13 after 100 hours of production.

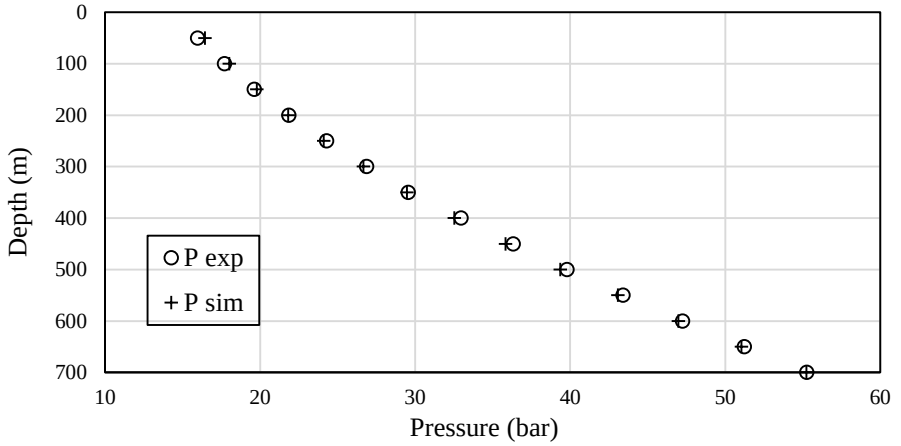


**Figure 12:** Comparison between experimental data and simulation results for the flowing pressure profile of the wellbore KD13 after 100 hours of production.

### 4.3.2 Application of T2Well for the interpretation of well-tests

To validate the capacity of T2Well-EWASG to simulate coupled wellbore-reservoir flow in geothermal systems and its application for the interpretation of well-tests, a full coupled wellbore-reservoir simulation was executed. This application deals with the interpretation of well-tests related to well WW-01, a productive slim hole drilled in the Wotten Waven Field, Roseaux Valley, Commonwealth of Dominica (ELC, 2013; Osborne et al., 2014). WW-01 is a vertical slim hole 1200 m deep and producing from a liquid-dominated reservoir. The maximum temperature and pressure, measured under shut-in conditions, are 238°C and 102 bar, respectively.

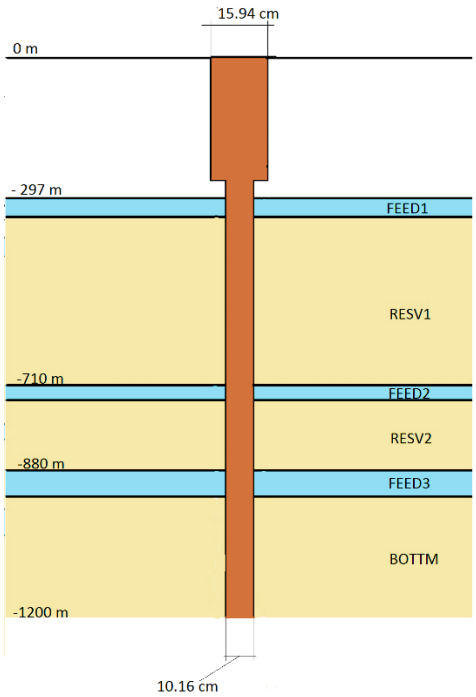


**Figure 13**: Conceptual model of the WW-1 well-reservoir system: well WW-1 and formation.

The developed WW-01 well-reservoir model (see Figure 13) consists in the cap-rock from 0 to -230 m (elevation referred to the ground), the first feed

zone located between -297 m and -344 m (FEED1), a reservoir layer between-344 m and -710 m (RESV1), the second feed zone between -710 m and -734 m (FEED2), the second reservoir layer between -734 m and -880 m (RESV2), the third feed zone between -880 m and -940 m (FEED3). The model is completed by a low permeable rock domain (BOTTM) below the third feed zone. The well is characterized by a change in diameter at - 263 m. At this depth the diameter change from a value equal to 7" ( internal diameter 15.94 cm) to a value equal to 4 ½" (internal diameter 10.16 cm). The numerical model is represented by a 2D radial grid with the wellbore along the axis of symmetry and which extends up to an outer radius of 1500 m, for a total number of 1658 elements.

Figure 14 shows a vertical cross section of the model in which the main feed zones can be identified (in yellow, green and cyan lighter colour). The cap-rocks has not been included in the model: the heat exchange between wellbore and the formation between 0.0 m and – 297 m has been simulated adopting the analytical approach.

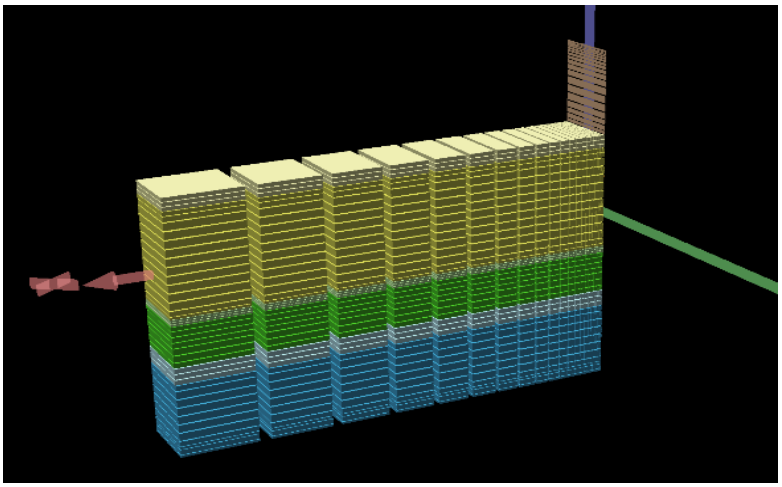

**Figure 14:** 2D vertical section of WW-01 wellbore –reservoir model. The main feed zones are the one with the lighter colors (yellow, green and cyan colors). The visualization of the model is performed by TOUGH2Viewer (Bonduà et al., 2012)

Figure 15 shows the shut-in temperature and pressure logs measured in WW-01 which could be reasonably close to reservoir natural state and then adopted as initial conditions for the steady state simulation (initial T and initial P of the well). In order to better replicate the recorded flowing temperature measurements the formation temperature assigned for the production simulation corresponding to FEED2 and FEED3 has been modified (Figure 15), and used as matching parameters. This suggests that the shut-in T log measurement may have been performed too early, without allows the system to stabilize after the perturbations due to drilling operations and completion tests.

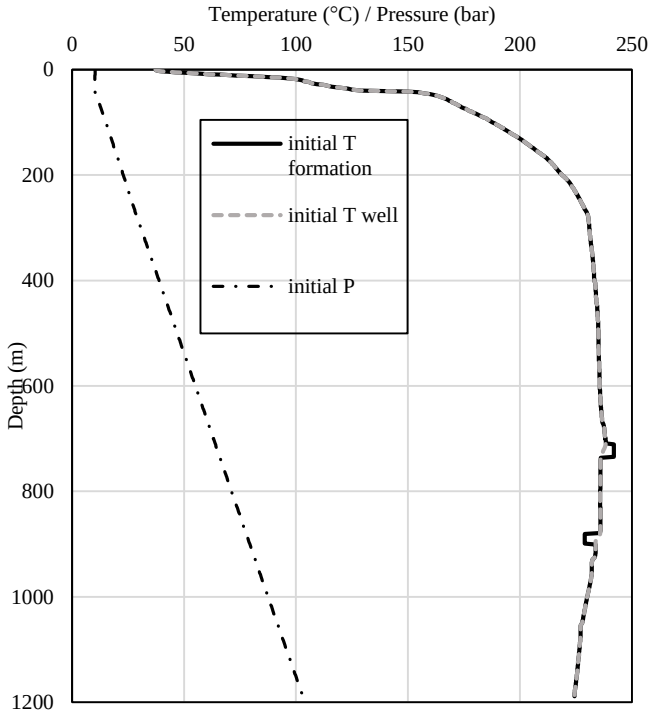


**Figure 15:** Initial pressure and temperature conditions assumed for the wellbore-reservoir model.

The production history (see Table 3) has been set using a time dependent fluid extraction from the top element of the wellbore grid, by furnishing the rate changes with time in the input. In Table 3 the total flow rate, the well head pressure (WHP), and the fluid specific enthalpy are listed along with time.

The history matching process requires the reproduction of experimental data by simulating the production history. Since this is the first application of T2Well-EWASG for the interpretation of WW-01 well-tests, a simplified scenario has been considered in which the contribution to the production is only due to FEED2 and FEED3, neglecting the possible contribution of FEED1.

**Table 3**: Production history of wellbore WW-01.

| Time | Total flow (kg/s) | WHP (bar) | Specific Enthalpy (kJ/kg) |
|---|---|---|---|
| 08:55 | | 4.5 | |
| 09:05 | 31.25 | 18.0 | 1087.63 |
| 09:14 | 26.89 | 18.0 | 1124.84 |
| 09:25 | 26.26 | 17.8 | 1236.6 |
| 09:45 | 25.55 | 17.8 | 1280.37 |
| 10:00 | 24.53 | 17.9 | 1222.65 |
| 10:15 | 22.65 | 17.9 | 1170.44 |
| 10:30 | 27.27 | 17.5 | 1289.96 |
| 11:18 | 24.99 | 17.5 | 1331.94 |
| 11:40 | 27.28 | 17.5 | 1230.11 |
| 12:25 | 25.01 | 17.5 | 1292.22 |
| 12:45 | 28.72 | 17.5 | 1162.59 |
| 12:55 | 26.00 | 17.9 | 1222.56 |
| 13:15 | 27.09 | 17.9 | 1178.11 |
| 13:50 | 28.6 | 17.8 | 1155.87 |
| 14:15 | 27.05 | 17.7 | 1155.23 |
| 14:45 | 16.77 | 19.4 | 1147.69 |
| 14:55 | 17.32 | 20.2 | 1094.99 |
| 15:05 | 16.44 | 20.2 | 1168.71 |
| 15:25 | 16.31 | 20.2 | 1156.68 |
| 15:45 | 17.15 | 20.3 | 1105.02 |
| 16:02 | 8.25 | 20.8 | 1155.98 |
| 16:15 | 8.03 | 20.8 | 1184.1 |
| 16:30 | 8.03 | 20.8 | 1184.1 |
| 18:00 | 0.00 | | |

Figure 16 displays the comparison between the assumed step wise production history and available field measurements

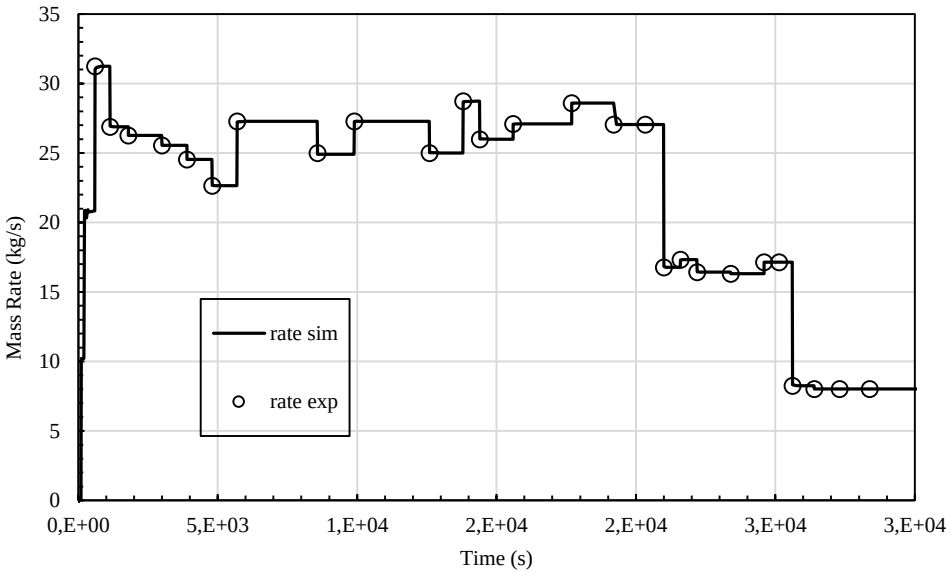


**Figure 16**: Comparison between simulated and measured mass rate.

.The experimental data available consists in two downhole flowing pressure transients at depths of 800 m and 1180 m, one flowing pressure and temperature log, well-head pressure, (WHP) and enthalpy. The permeability of different rock domains were calibrated in order to reproduce the experimental results and in Table 4 the results of the calibration of the model are listed. For this preliminary study, possible skin effects for both producing feed zones have been neglected.

**Table 4**: Reservoir formation permeability (horizontal) as obtained by model calibration.

| **rock type** | **perm XY ($m^2$)** |
|---|---|
| FEED1 | $15*10^{-15}$ |
| RESV1 | $1.5*10^{-15}$ |
| FEED2 | $150*10^{-15}$ |
| RESV2 | $0.5*10^{-15}$ |
| FEED3 | $30*10^{-15}$ |
| BOTTM | $0.02*10^{-15}$ |

As showed in Figure 17 the measured flowing pressure profile and the simulated one are in good agreement. Figure 18 shows the comparison of recorded and simulated temperatures. The percentage difference value is about 0.37% for the temperature and it is about 2.12% for the pressure.

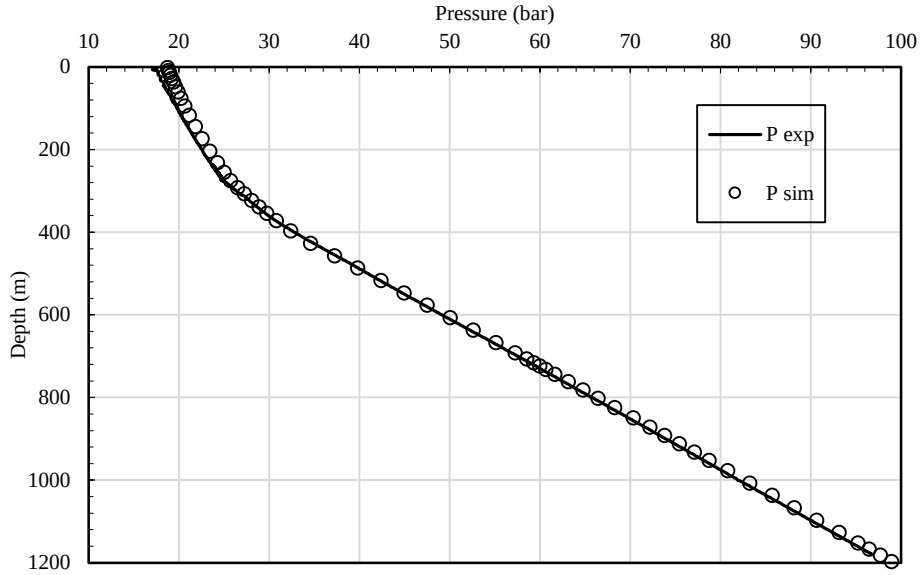


**Figure 17:** Comparison between measured and simulated flowing pressure. The two set of data show a fairly good agreement.

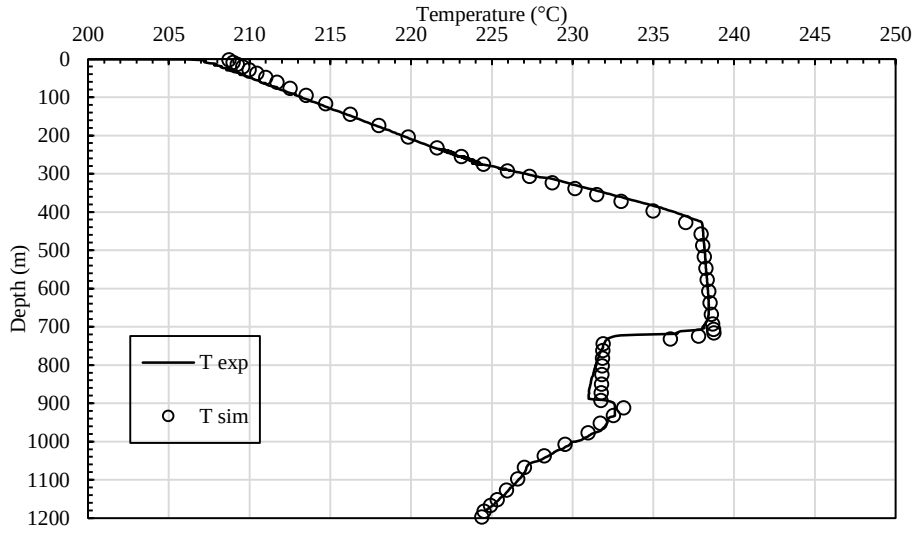


**Figure 18:** Comparison between measured and flowing simulated temperature. The two sets of data show a good agreement.

In Figure 19 pressures recorded at 800 m, 1180 m and at wellhead are compared with the simulated results. From the plots it is clear that the agreement between recorded and simulated pressure is reasonably good, while the WHP is underestimated after 21,000 s.

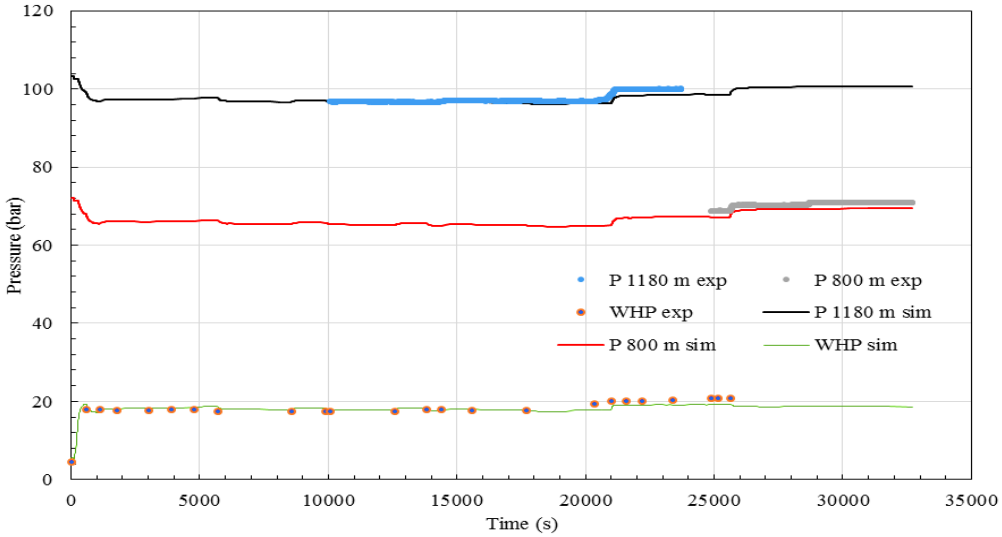


**Figure 19:** Flowing downhole pressure (800m and 1180 m depth) and WHP: simulated results compared with field measurements.

Figure 20 shows the comparison between the production enthalpy listed in Table 3 and the numerical simulation results. The simulated enthalpy values show a constant value of about 1011 kJ/kg. This result is in agreement with the production from a liquid dominated geothermal reservoir however the simulated results underestimate experimental data of a quantity ranging between 150 kJ/kg and about 50 kJ/kg.

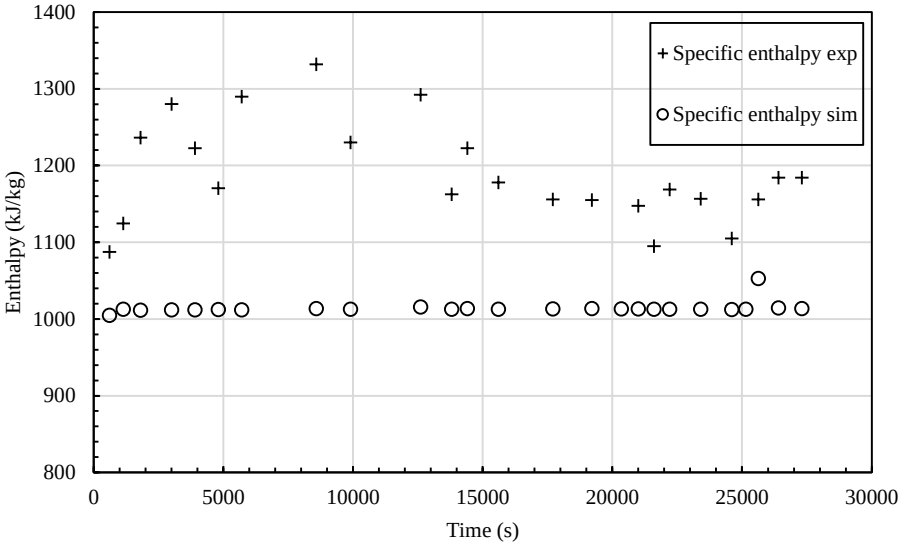


**Figure 20** Measured and simulated production enthalpy.

ELC Electroconsult (2013) has already mentioned the higher enthalpy estimated from field data. The difference between simulated and experimental data could be caused by either:

- measurements errors during the production tests;

and/or:

- the contribution of the first feed zone which is neglected in the present model.

In this study, the calibration of the formation parameters is performed, in particular, on the horizontal permeability of FEED2 and FEED3, with the aim to get a better match between the field data and simulation results without trying to replicate the behaviour of all the feed zones in details. The contribution of the first feed zone will be the objective of further study. Since the first feed zone, FEED1, is in two-phase conditions it could then increase the production enthalpy by contributing with a two-phase mixture with excess steam with respect to the static feed temperature. Finally, Figure 21 shows the comparison between the simulated and experimental output curves (Rate vs

WHP). The agreement between the results is good at rates under 20 kg/s but at higher rates the simulated WHP overestimates the measured values.

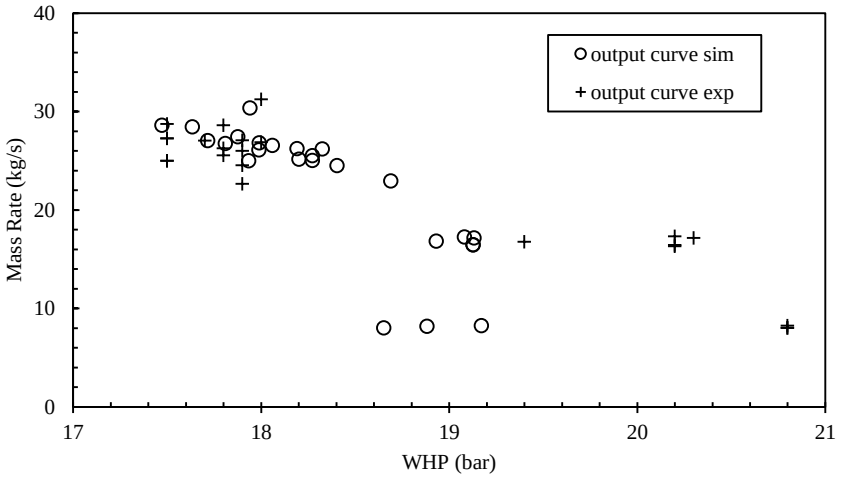


**Figure 21**: Output curve: comparison between simulated results and measured data.

It is reasonable to consider that, since the WHP is linked to the production enthalpy, the production enthalpy could actually be higher than the simulated one due to the contribution of higher enthalpy fluid from the upper feed (FEED1) neglected in this preliminary study.

# 5 Application of TOUGH2Viewer and VORO2MESH

In this chapter, the results obtained after applying TOUGH2Viewer and VORO2MESH in a case study related to the gas migration in deep sedimentary formation are described. The case study allowed to test VORO2MESH in creating fully 3D Voronoi grids and the updated version of TOUGH2Viewer which is able to visualize fully 3D Voronoi grids.
This activity was part of a project named "Gas System", between DICAM, eni SpA and Saipem, which took place from 16 July to 15 December 2014 (first part) and from 27 May and 17 July 2015 (second part). The project refers to the improvement of simulation techniques used for modelling the migration of NCG in sedimentary formations during the basin evolution, at basin scale and for geological times.
The results have been presented at the TOUGH Symposium, LBNL, California, 28-30 September 2015 [Bonduà et al., 2015].

TOUGH2Viewer and VORO2MESH have been mainly tested through the numerical modelling of the following case study. The case study deals with the migration of non-condensable gases (NCG) in a large sedimentary formation bounded between two geological surfaces. The simulation has been executed using an enhanced version of TOUGH2-TMGAS (Battistelli and Marcolini, 2009). The simulations have been performed using two different

grids, a structured grid and a 3D Voronoi grid. Both were created with VORO2MESH and the simulations results were analysed with TOUGH2Viewer.

## 5.1 TMGAS EOS MODULE

TMGAS is an EOS dedicated to the thermodynamic description of multi-phase mixture of NK components such as water, brine, inorganic gases ($CO_2$, H2S and N2) and hydrocarbons. It has been realized to model the injection of mixtures of inorganic gases and hydrocarbons in geological structure, situation typically found, for example, in natural gas storage operations, $CO_2$ injection into saline aquifer and enhanced oil recovery. The components of the mixture can be present in two fluid phase: the non-aqueous phase (gas, supercritical or condensed conditions) and the aqueous phase (dissolved hydrocarbons and gases in water with dissolved solids like NaCl). The salt can precipitate determining the formation of a solid phase. The code is able to determine the passage from a thermodynamic state to another by identifying the phase condition for each grid block at each Newton-Rapson iteration. Starting form single non–aqueous phase, aqueous phase evolves if the sum of molar fractions of the hypothetical aqueous phase in equilibrium with the non-aqueous phase becomes greater than one. In the same manner the appearance of non-aqueous phase from single aqueous phase is managed. In two phase condition the disappearance of a phase is recognized by the value of its saturation, which becomes negative. The precipitation of halite occurs when the NaCl concentration exceeds the equilibrium solubility. The formulation of water, brine and halite properties are the same of EWASG. For further details, the reader is referred to the paper of Battistelli and Marcolini, 2009.

## 5.2 Model and Grids description

The portion of the studied basin occupies an area of about 25,000 km$^2$ and it is characterized by an average thickness of 800 m. Figure 22 displays a schematic top view of the model: the NCG injection is set in a cluster of blocks located at the bottom left and the outlet block is set at the top left corner (green circle in Figures 22).

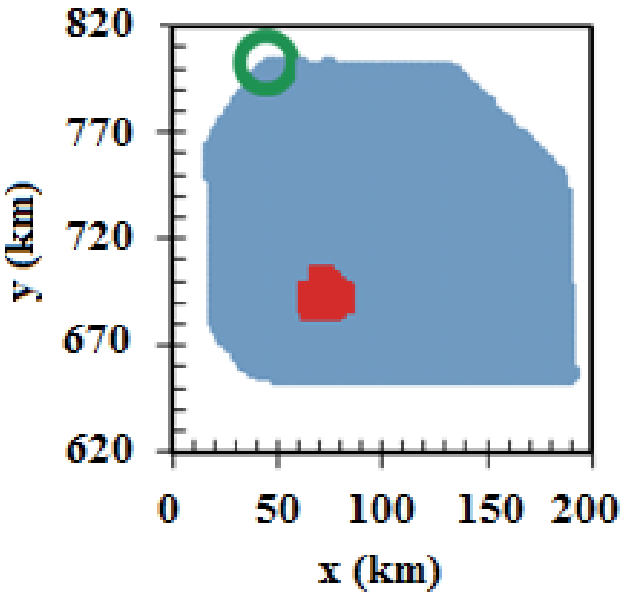


**Figure 22:** 2D view of the gridded surface. Highlighted in red colour the position of the cluster of injection blocks. In green, the boundary block used as outlet of the system.

Both grid created represent the geological formation which is characterized by an elevation from -2000 m down to -7000 m above sea level. The boundary surfaces of the domain have been provided as grids (x, y, z, points file) with a resolution of 1700 × 1700 m$^2$, covering 180,000 m along X and 146,000 m along Y. The discretization of the volume between the two boundary surfaces is obtained applying the Voronoi approach near the surface allowing a realistic representation of the surface itself and, at the same time, limiting the number of blocks by discretizing the remaining region far from the surfaces with a regular grid with blocks of 1700 × 1700 × 140 m$^3$.

A convex hull enveloping the whole domain has been used in order to define the domain formation volume to be discretized. Furthermore, the domain has

been cut with vertical planes in order to remove the regions of no interest. Figure 23 displays the resulting 3D grid as it can be visualized by TOUGH2Viewer.

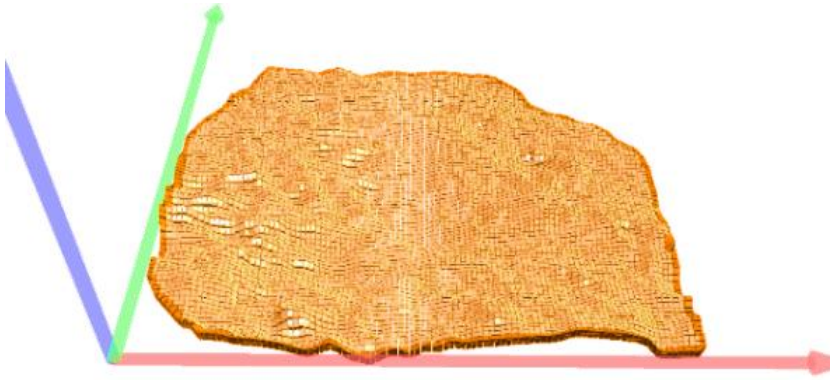

**Figure 23:** The 3D Voronoi grid (vertical exaggeration 5×), visualization by TOUGH2Viewer.

In Figure 24, a portion of the 3D Voronoi grid with the two geological boundary surfaces (purple wireframe) are shown. In particular, looking in to the section, it is possible to distinguish the regular blocks and the Voronoi ones. The last Voronoi layer, used near the surface, allows a greater improvement in the representation of the surface itself.

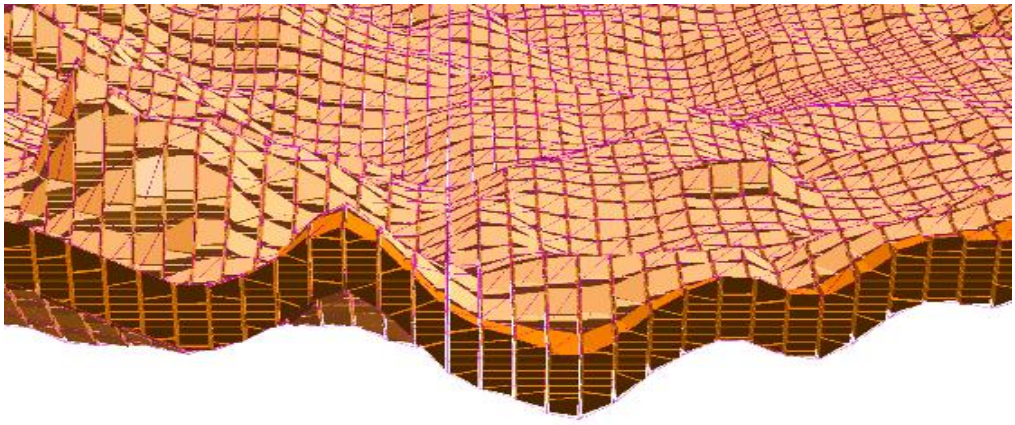

**Figure 24:** Grid and surfaces (purple wireframe) representing geological upper and bottom limits (vertical exaggeration 5×), visualization by TOUGH2Viewer.

Figure 25 (obtained with Paraview using a data set exported by TOUGH2Viewer) shows a comparison between the same local maximum (a structural high) discretized with the two different grids: the structured grid in Figure 25a and the 3D Voronoi grid in Figure 25b.

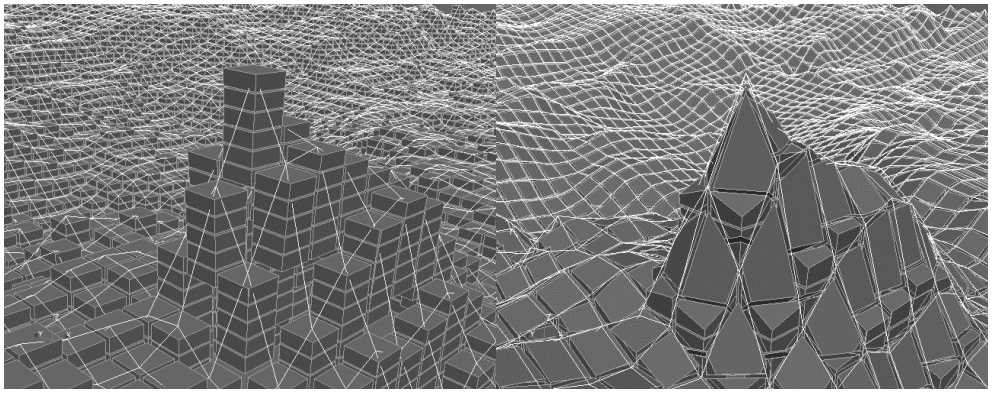

(a) (b)

**Figure 25:** The same region gridded with: (a) regular discretization; (b) 3D Voronoi tessellation. The white wireframe represents the geological boundary surface (vertical exaggeration 5×), visualization by Paraview.

From this comparison it is evident that 3D Voronoi grid can represent the geological surface shape (white wireframe) with a better fit and greater modelling accuracy. In particular, this feature is more advantageous as the geological domain shape is full of heterogeneities. In Table 5, a comparison of the main characteristics of the two grids is listed. The structured grid has been realized in the domain between the two geological surfaces, cutting the negligible regions as has been done for the 3D Voronoi grid. It is characterized by blocks of 1700×1700×140 $m^3$.

**Table 5**: Comparison of main characteristics of the regular structured grid and the 3D Voronoi grid. Volumes are in $m^3$ and areas in $m^2$.

| | **Regular model** | **3D Voronoi model** |
|---|---|---|
| **Number of blocks** | 48482 | 36258 |
| **Min Volume blocks** | $1.5172*10^8$ | $3.128*10^8$ |
| **Max Volume blocks** | $6.069*10^8$ | $1.9197*10^9$ |
| **Total Volume** | $1.9465*10^{13}$ | $1.9528*10^{13}$ |
| **Mean Volume** | $4.0148*10^8$ | $5.386*10^8$ |
| **Number of connections** | 122610 | 192186 |
| **Min num. connections** | 1 | 6 |
| **Max num. connection** | 6 | 25 |
| **Min connection area** | 1141.4 | 1.0 |
| **Max connection area** | $4.335*10^6$ | $7.225*10^6$ |

## 5.3 Simulation results

The case study deals with the simulation of the gas migration over a time of $10^6$ years. The generation of NCG has been simulated by providing a constant injection of gas. Figure 26 shows the saturation of the NCG at the end of the simulation (obtained with Paraview) for the structured grid (Figure 26a) and for the 3D Voronoi grid (Figure 26b). Comparing the two results it is possible to verify that, since the 3D Voronoi grid better reproduces the geological shape of the formation, in the Voronoi grid the NCG accumulation is more localized in structural highs. In structured grids (Figure 26a) the NCG plume is less localized.

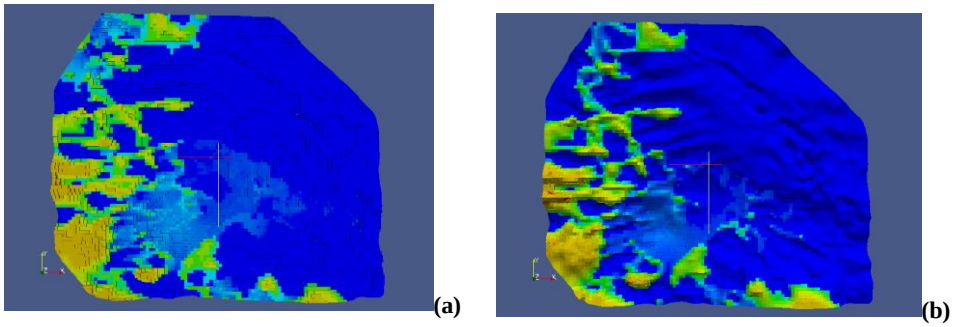

**(a)** **(b)**

**Figure 26:**Top view of non-aqueous phase saturation $S_{NA}$ after $10^6$ years of $CO_2$ injection: (a) regular structured grid; (b) 3D Voronoi grid, as plotted by Paraview.

Analysing the total volume of injected NCG along with the time it is possible to highlight additional differences between the simulation performed with the structured and with the 3D Voronoi grid (see Figure 27). In particular, the different tendency of the two curves after about 2 $10^{13}$ s, is due to the fact that in the 3D Voronoi grid simulation the NCG arrives at the outlet boundary block earlier than that in the regular structured grid.

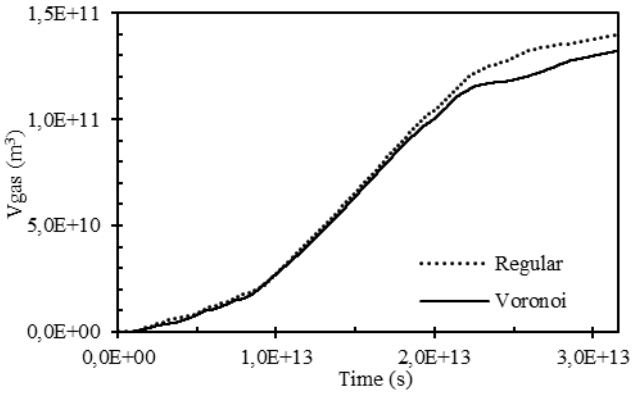


**Figure 27:** Comparison of simulation results: total volume of gas vs time.

Figure 28 shows the number of time steps along with the simulated time.

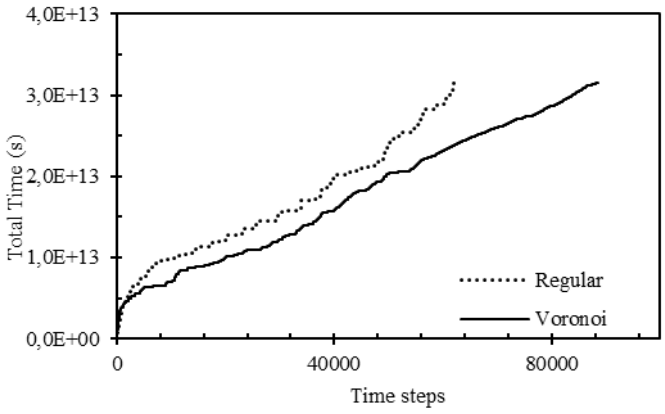


**Figure 28:** Comparison of simulation results: time steps vs. total simulated time.

To reach the simulated time, $10^6$ years, the regular structured grid required 62,605 time steps while the 3D Voronoi grid needs 88,454 time steps. The

computation time, using a PC furnished with a processor Intel® Core™ i7-3770K CPU @ 3.50 GHz, with 8 GB RAM, for the 3D Voronoi grid was 182% of that required by the regular grid. It is clear that the use of a 3D Voronoi grid, which has an increased number of connections, increases the cost of computations.

Furthermore, the higher number of connections further intensifies the rise of the problems associated with the appearance/disappearance of the non-aqueous (NA) phase present in these simulations.

Using a 3D Voronoi grid, the simulation better reproduces the NCG migration and its accumulation in structural highs. In particular, this study allowed to underline the better performance of 3D Voronoi grids in geological shape reproduction. Referring to the two-phase flow, the better reproduction of geological structural highs becomes fundamental as it allows modelling the NCG migration and accumulation distribution in the geological formation in a more realistic way.

# 6 Conclusions

## 6.1 TOUGH2Viewer and VORO2MESH application

The application of VORO2MESH and TOUGH2Viewer to a case study dealing with the migration of NCG in deep sedimentary formation, allowed to assess the different simulation results and computational times obtained using a regular structured grid and a 3D Voronoi grid. The Voronoi approach permits to build grids according with the IFDM and to better reproduce the shapes of geological formations. As the heterogeneity of the geological formation increases, this feature becomes more important. At the same time 3D Voronoi grids must be carefully generated because even if considering a simulation volume discretized with a comparable number of blocks as in a regular structured grid, the number of connections can increase drastically, thereby affecting the computational time of the simulation.

Since 3D Voronoi grids are complex both in creating and in managing, they can be properly adopted only if adequate pre- and post-processing tools are available. The results of this study demonstrate that VORO2MESH and TOUGH2Viewer are capable of dealing with full 3D unstructured grids, from their creation to results visualization.

## 6.2 T2Well-EWASG

In order to enhance the reservoir engineering activities, it has been decided to use the software T2Well for a more accurate interpretation of well-tests in

geothermal reservoirs. Since up to now, T2Well has primarily been used in carbon sequestration studies, it has been necessary to couple T2Well with the EOS EWASG, which describes the typical thermodynamic condition in high enthalpy geothermal reservoir. Furthermore, the computation of analytical heat exchange between the wellbore and the formation has been enhanced, taking into account the thermal resistivity of the completion. T2Well-EWASG has been realized and tested (verification and validation).T2Well-EWASG has been verified in order to check the results of the modified analytical heat exchange approach. The validation has been performed by simulating flowing P&T logs reported in the literature, as well as by interpreting a short production test performed on a high enthalpy geothermal well. In particular, the latter application proves that T2Well-EWASG can be used for integrated interpretation of surface and downhole measurements collected during the performance of production tests in geothermal wells.

In order to highlight the relevance of T2Well-EWASG as interpretation tool for geothermal well-tests, and referring to the WW-01 case study, it is important to point out that even if we would not have access to any flowing pressure and temperature profile, we could in any case match the experimental WHP with the simulated one and the comparison would show the enthalpy differences. This is possible because usually WHP and enthalpy measurements are always done. The strength of this tool, however, is not to reduce uncertainty of the results, but is that it allows to reduce the different possible solutions (in terms of reservoir characteristics) within an acceptable error, by allowing to interpret surface and downhole measurements in conjunction, instead of separately [Battistelli, 2016]. From this point of view T2Well-EWASG can be effectively used as a tool which allows an optimization of reservoir engineering activities.

## 6.3 Future Work

In this section the possible future development of the research topic of the present thesis are presented.

### 6.3.1 Inverse simulation

The parameters calibration done in the WW-01 case study was done by trial-and-error. An important step forward would be the use of inverse simulation techniques to improve the calibration of the model. In this way could be possible to determine the hydraulic properties of the formation not only by rocks type, as it has been realized in this study, but it could be also determined the heterogeneity of the formation, i.e. hydraulic properties cell by cell.

To do this it is necessary to apply an automatic inverse simulation, which could be done using PEST [Doherty, 2005] or, better, integrating T2Well into iTOUGH2, or using the PEST protocol implemented in iTOUGH2 [Finsterle, 2011]. Since PEST has been created in order to make the inverse simulation, in this case it is not necessary to modify the T2Well-EWASG code. PEST will change the model parameters, by rewriting the input file for T2Well, and then run the simulation until the results will satisfy the required objectives. The option related to integrating T2Well into iTOUGH2 requires important modifications of the T2Well code since iTOUGH2, for example, manages the common variables in a different way (by include files).

### 6.3.2 Analytical computation of heat exchange

In this study, the analytical computation of heat exchange between the wellbore and the formation has been enhanced by extending its validity to each time and by introducing the over-all heat transfer coefficient which

allows to take into account the thermal resistivity of the completion of the wellbore. The implemented analytical solution is valid only if the temperature inside the wellbore is constant. In order to take into account the changes in wellbore temperature it is necessary to apply the superposition of effects as done by Zhang et al., 2011. In their work, they find a relation to compute the heat exchange between the wellbore and the formation which is a time-convolution result of the variation of temperature of the wellbore wall. In our case it is necessary to obtain the expression of the time-convolution taking into account the thermal resistance related to well completion and, as explained by Zhang et al. 2011, it is necessary to modify the code in order to store the temperature history of each wellbore cell.

### 6.3.3Non-Darcy flow near the wellbore

In order to enhance the performance of the model, it could be useful to take into account of non-Darcy flow in the neighbourhood of the wellbore. It is well known that near the well region during high flow rate the laminar flow condition is not more satisfied, so the non-Darcy effect is predominant. This has been recognized in gas and oil fields but also in liquid flow in geothermal reservoir [Zhang and Xing, 2012]. As pointed out by Zhang and Xing, 2012, the interpretation of well-tests assumes the validity of Darcy's law and this means that the pressure gradient and the linear velocity of fluid flow are in a linear relation. But near the wellbore, this assumption is not valid any more. For example, Holditch and Morse, 1976, studying the gas well productivity, pointed out that the non-Darcy effect greatly reduces the gas productivity and affects the determination of hydraulic properties. From this point of view, the introduction of the computation of non-Darcy flow, for example, by Forchheimer equation [Forchheimer, 1901], could result in a more reliable

match between experimental data and simulation results, leading the reservoir engineer to more reliable considerations.

# References

Alcott, A., Swenson, D., Hardeman, B., *Using PetraSim to create, execute, and Post-Process TOUGH2 models*, Proceedings of TOUGH Symposium 2006, Lawrence Berkeley National Laboratory, Berkeley, California. May 15-17.

Aurenhammer, F., Voronoi Diagrams – A survey of a fundamental geometric data structure, ACM Computing Surveys, Vol. 33, No, 3, September 1991.

Axelsson, G., and Stefansson, V., 2003, Sustainable management of geothermal resources, InProceedings of the International Geothermal Conference, Reykjavík, Iceland, September 2003.

Axelsson, G., 2013, Geothermal well testing, Presented at "Short Course V on Conceptual Modelling of Geothermal Systems", organized by UNU-GTP and LaGeo, in Santa Tecla, El Salvador, February 24- March 2, 2013.

Avis, J., Calder, N.,Walsh, R., 2012. *MVIEW e a powerful pre- and post-processor for TOUGH2*, Proceedings, TOUGH Symposium 2012, Lawrence Berkeley National Laboratory, Berkeley, California. Sept. 17-19 1996.

Barelli, A., Corsi, R., Del Pizzo, G. and Scali, C., A two-phase flow model for geothermal wells in the presence of non-condensable gas, *Geothermics*, Vol.11, No.3, pp.175-191, 1982.

Battistelli, A., Calore, C., Pruess, K., The simulator TOUGH2/EWASG for modelling geothermal reservoirs with brines and a non-condensible gas. Geothermics, Vol. 26, No. 4, pp. 437-464, 1997.

Battistelli, A., Nagy, S., Reservoir engineering assessment of low-temperature geothermal resources in the Skierniewice municipality (Poland), Geothermics, 29, 701-721, 2000.

Battistelli, A., Yiheyis, A., Calore, C., Ferragina, C., Abatneh, W., Reservoir engineering assessment of Dubti geothermal field, Northen Tendaho Rift, Ethiopia, Geothermics, 31, 381-406, 2002.

Battistelli A., 2004, Modelling biodegradation of organic contaminants under multiphase conditions with TMVOCBio. Vadose Zone Journal, Vol. 3, n.3, 875-883.

Battistelli A., Marcolini M. (2009). TMGAS: a new TOUGH2 EOS module for the numerical simulation of gas mixtures injection in geological structures. Intl. J. Greenhouse Gas Control, 3, p. 481-493.

Battistelli, A., Improving the treatment of saline brines in EWASG for the simulation of hydrothermal systems, In: Proceedings of TOUGH Symposium 2012. Lawrence Berkeley National Laboratory, Berkeley, California. September. 17-19, 2012.

Battistelli A., Marcolini M., 2012, personal communication.

Battistelli A., 2013, personal communication.

Battistelli A., Berry P., Bonduà S., Bortolotti V., Consonni A., Cormio C., Geloni C., Vasini E.M., 2015,Thermodynamics related processes during the migration of acid gases and methane in deep sedimentary formations. TOUGH Symposium 2015, Berkeley, California September, 28-30, 2015.

Battistelli, A., 2016, personal communication.

Berry, P., Bonduá, S., Bortolotti, V., Cormio, C., Vasini, E.M., 2014, A GIS-based open-source pre-processor for georesources numerical modeling, Environmental Modelling and Software, Volume 62, December 2014, Pages 52–64.

Bertani, R., 2015, Geothermal Power Generation in the World 2010-2014 Update Report. Proceedings World Geothermal Congress 2015, Melbourne, Australia, 19-25 April 2015.

Bhat, A., Swenson, D. and Gosavi, S. (2005). Coupling the HOLA Wellbore Simulator with TOUGH2. In Proceedings of the 30th Workshop on Geothermal Reservoir Engineering Stanford University, Stanford, California, USA.

Björnsson, G., 1987, A Multi-Feedzone Geothermal Wellbore Simulator. Berkeley, University of California, USA.

Blanco Martìn L., Rutquist J., Birkolzer J., Battistelli A., 2015, Long-term modeling of coupled processes in a generic salt repository for heat-generating nuclear waste: preliminary analysis of the impacts of halite dissolution and precipitation. 49th US Rock Mechanics / Geomechanics Symposium, San Francisco, CA, USA, 28 June- 1 July 2015.

Bodvarsson, G.S., 1982, Mathematical modeling of the behavior of geothermal systems under exploitation, PhD. Thesis, Lawrence Berkeley Laboratory, University of California.

Bonduà, S., Berry, P., Bortolotti, V., Cormio, C., 2012, TOUGH2Viewer: A post-processing tool for interactive 3D visualization of locally refined unstructured grids for TOUGH2, Computer & Geosciences, 46, pp. 107-118.

Bonduá, S., Battistelli, A., Berry, P., Bortolotti, V., Consonni, A., Cormio, C., Geloni, C., Vasini E.M., 2015, 3D Voronoi pre- and post- processing tools for the modeling of deep sedimentary formations with the TOUGH2 family of codes, Proceedings, TOUGH Symposium 2015, Lawrence Berkeley National Laboratory, Berkeley, California, September 8-30, 2015.

Bortolotti, V., 2013, Lectures on Numerical Simulatons of Acquifer, Lectures notes.

Brennen, C.E., 2005, Fundamentals of multiphase flows. Cambridge University Press, pp.34-35.

Burnell, J.G., White, S.P., Osato, K., Sato, T., May 12-14, 2003. GeoCad, a pre- and postprocessor for TOUGH2.In: Proceedings, TOUGH Symposium 2003.Lawrence Berkeley National Laboratory, Berkeley, California, USA.

Calore, C., Battistelli, A., 2003, Application of TOUGH2/EWASG to the modelling of salt water injection into a depleted geothermal reservoir: preliminary results. Proceedings, TOUGH Symposium 2003, Lawrence Berkeley National Laboratory, Berkeley, California, May 12-14, 2003.

Carslaw, H.C., and Jaeger, J.C., 1959, Conduction of heat in solids, second edition, oxford University press.

Chou, I. M., 1987, Phase relations in the system NaC1-KC1-H20. III: solubilities of halite in vapor-saturated liquids above 445°C and redetermination of phase equilibrium properties in the system NaCI-H20. Geochimica et Cosmochimica Acta 51, 1965-1975.

Crestaz E., Adames H., Battistelli A., Chersicla A., Rodriguez H., Suppo M., Tabani L., 2002, The Planicie Costera Oriental coastal aquifer (Dominican Republic). A general framework analysis supported by conceptual groundwater modelling. XIV Intl. Conference on Computational Methods in Water Resources, Delft, The Nederlands, 23-28 June, 2002, p. 546-554.

Croucher, A., PyTOUGH: a Python scripting library for automating TOUGH2 simulations, Proceedings of the New Zealand Geothermal Workshop 2011, Auckland, New Zealand, 21-23 November 2011.

Croucher A.E., and M.J. O'Sullivan, Application of the computer code TOUGH2 to the simulation of supercritical conditions in geothermal systems. Geothermics, 37, 622–634, 2008.

DiPippo R., "Geothermal Power Plants. Principles, Applications, Case Studies and Environmental impact", chapter 4, Second Edition, 2008, Elsevier.

Doherty, J., 2005, PEST, Model-Independent Parameter Estimation, User Manual 5th Edition, Watermark Numerical Computing.

Driesner T., The system H2O–NaCl. Part II: Correlations for molar volume, enthalpy, and isobaric heat capacity from 0 to 1000°C, 1 to 5000 bar, and 0 to 1 XNaCl. Geoc. Cosm. Acta, 71, 4902–4919, 2007.

ELC Electroconsult, Wotten Waven Geothermal Field, Commonwealth of Dominica, West Indies: Feasibility Study. Report for the Ministry of Public Utilities, Energy and Ports, Commonwealth of Dominica, 2013 (*unpublished*).

Esposito, A., Augustine, C. (2014). Results of Reservoir Modeling of the Operation and Production of a Recompleted Gas Well in a Geopressured/Geothermal Reservoir in the Wilcox Formation, Texas, for Electricity Generation. Society of Petroleum Engineers, paper SPE-169902-PA.

Falta, R.W., Pruess, K., Finsterle, S., and Battistelli, A., 1995, T2VOC User's Guide, Lawrence Berkeley Laboratory Report LBL-36400, March

Faust, C.R., and Mercer, J.W., 1977, Version I - A finite-difference model of two dimensional,single- and two-phase heat transport in a porous medium: U.S. Geological Survey Open-File Report 77-234, 84.

Finsterle, S. 2007. iTOUGH User's Guide, Earth Science Division, Lawrence Berkeley National Laboratory, University of California, Berkeley, CA 94720.

Finsterle, S., Sonnenthal E.L., Spycher, N., 2014, Advance in subsurface modeling using the TOUGH suite of simulators, Computer & Geoscience, 65 2-12.

Flint A.L., Ellett K.M., 2003, The Role of the Unsaturated Zone in Artificial Recharge at San Gorgonio Pass, California. Vadoze Zone Journal, V.3, n. 3, p. 763-774.

Forchheimer, P., 1901, Wasserbewegung durch Boden. Zeits. V. Deutsch. Ing. 45,1782–1788.

Freeston, D., Gunn C., 1993. Wellbore simulation-case study, Proceedings of the Eighteenth Workshop on Geothermal Reservoir Engineering Stanford University, Stanford, California, January 26-28, 1993.

Geloni C., Battistelli A. (2010). Modelling the injection of mine drainage groundwater in a vapor dominated geothermal reservoir: preliminary evaluation of permeability damage risks. Consoil 2010, Salzburg, 22-24 September 2010.

Grant M.A., Bixley P.F., 2011, Geothermal reservoir engineering, second edition, Academic Press, Burlington, USA.

Gudmundsdottir, H., Jonsson, M.T., and Palsson H., 2012, A coupled wellbore-reservoir simulator utilizing measured wellhead conditions, Proceedings 53rd SIMS Conference on Simulation and Modeling, The National Energy Authority (NEA), Reykjavik, October 3-6 2012.

Gudmundsdottir, H., Jonsson, M.T., 2015. The Wellbore Simulator FloWell – Model Enhancement and Verification. Proceedings World Geothermal Congress 2015, Melbourne, Australia, 19-25 April 2015.

Gunn C. and Freeston D., 1991, An Integrated Steady-State Wellbore Simulation and Analysis Package. In Proceedings of 13th New Zealand Geothermal Workshop, Auckland, New Zealand.

Hagdu T., Zimmerman R. and Bodvarsson G., 1995, Coupled Reservoir-Wellbore Simulation of Geothermal Reservoir Behavior. Geothermics, 24(2):145-166.

Haas Jr, J. L., 1976, Physical properties of the coexisting phases and thermochemical properties of the H2O component in boiling NaCI solutions. USGS Bulletin 1421-A.

Hayba, D.O., Ingebritsen S.E. 1994. The computer model HYDROTHERM, a three-dimensional finite-difference model to simulate ground-water flow and heat transport in the temperature range of 0 to 1200 °C. U.S. Geological Survey, Water-Resources Investigations Report 94-4045. Reston, Virginia.

Hu, B., 1995, Reservoir simulation of the Yangbajian geothermal field in Tibet, China. In Proceedings of the World Geothermal Congress, Florence, Italy.

Hu, L., Pan, L., Zhang, K., 2012, Modelling brine leakage to shallow aquifer through an open wellbore using T2Well/ECO2N, International Journal of Greenhouse Gas Control, 9, pp. 393-401.

Hu, S., 1994, Distribuited parameter model for the Zhangzhou geothermal field, China, Geothermal training programme, Orkustofnun, Grensasvegur 9, Reykjavik, Iceland.

International Association for the Properties of Water and Steam, Release on the IAPWS Formulation 2008 for the Viscosity of Ordinary Water Substance. Berlin, Germany, 2008.

International Association for the Properties of Water and Steam, Release on the IAPWS Industrial Formulation 1997 for the Thermodynamic Properties of Water and Steam. Erlangen, Germany, 1997.

Itasca Consulting Group Inc., 1997, FLAC-3D Manual: Fast Lagrangian analysis of continua in 3 dimensions–Version 2.0. Itasca Consulting Group Inc., Minnesota, USA.

James, R., 1975, Gas content of a hot-water reservoir estimated from downhole pressure and temperature measurements. Second United Nations Symposium, Berkeley, CA. Vol. 3, pp. 1689-1691.

Kanev, K., Ikeuchi, J., Kimura, S. and Okajima, A., Heat loss to the surrounding rock formation from a geothermal wellbore, *Geothermics*, Vol. 26, No. 3, p. 329-349, 1997.

Lasseter, T. J., Witherspoon, P. A., and Lippmann, M. J., 1975, The Numerical Simulation of Heat and Mass Transfer in Multidimensional Two-Phase Geothermal Reservoirs, Proceedings, 2nd U.N. Symposium on Development and Use of Geothermal Resources, Vol. 3, p. 1715.

Li, Y., Niewiadomski, M., Trujillo, E., Sunkavalli, S.P., Tougher: a user-friendly grafical interface for TOUGHREAC, Comput. Geosci. 37 (6), 775-782, 2011.

Lorenz, S., Muller, W., Modelling of halite formation in natural gas storage aquifers. Proceedings, TOUGH Symposium 2003, Lawrence Berkeley National Laboratory, Berkeley, California, May 12-14, 2003.

Marcolini M., Battistelli A. (2012) Modeling of wellbore flow within geothermal reservoir simulations at field scale. Proceedings, TOUGH Symposium 2012, Lawrence Berkeley National Laboratory, Berkeley, California, Sept. 17–19, 2012.

Miller, C.W. (1980). Welbore User's Manual. Berkeley, University of California, Report, no. LBL-10910, USA.

Moridis, G.J., and Pruess, K., 2014, User's Manual of the TOUGH+ Core Code v1.5: a general-purpose simulator of non-isothermal flow and transport through porous and fractured media, Earth Science Division, Lawrence Berkely National Laboratory, CA 94720, LBNL-6871E.

Murray, L. and Gunn, C. (1993). Toward Integrating Geothermal Reservoir and Wellbore Simulation: TETRAD and WELLSIM. In Proceedings of the 15th New Zealand Geothermal Workshop, Auckland, New Zealand.

Newson, J., Mannington, W., Sepulveda, F., Lane, R., Pascoe, R., Clearwater, E., O'Sullivan, M. J., January 30 - February 1, 2012, Application of 3D modelling and visualization software to reservoir simulation: Leapfrog geothermal and TOUGH2. In: Proceedings, Thirty-Seventh Workshop on Geothermal Reservoir Engineering. Stanford University, Stanford, California, 2012, USA.

Notiziario UGI, La geotermia ieri, oggi e domani, numero speciale del notiziario UGI, Novembre 2007, Edizioni ETS.

Oldenburg, C.M., Freifeld, B.M., Pruess, K., Pan, L., Finsterle, S., Moridis, G.J., 2011, Numerical simulations of the Macondo well blowout reveal strong control of oil flow by reservoir permeability and exsolution of gas. Ed. Marcia K. McNutt, Proc. National Academy of Sciences of the United States of America, vol. 109, 50, p. 20254–20259 .

Oldenburg, C. M., Pan, L., Porous media compressed-air energy storage (PM-CAES): theory and simulation of the coupled wellbore reservoir system, *Transport in Porous Media*, DOI 10.1007/s11242-012-0118-6, 2013.

O'Sullivan, M.J. and Bullivant, D. P., 1995, A graphical interface to the TOUGH2 family of flow simulators, Proceedings of TOUGH Workshop 1995, Lawrence Berkeley Laboratory, Berkeley, CA, (1995).

O'Sullivan, M.J., Pruess, K., Lippman, M.J., 2001, State of art of gothermal reservoir simulation. Geothermics, 30, 395-429.

O'Sullivan, M.J., Yeh, A., Mannington, W.I., 2009, A history of numerical modelling of the Wairakei geothermal field, Geothermics, 38, 155-168.

Osborn, W., Hernández, J., George, A., 2014, Successful Discovery Drilling in Roseau Valley, Commonwealth of Dominica. Proc., 39th Workshop on Geothermal Reservoir Engineering Stanford U., Stanford, CA, Feb. 24-26, 2014 SGP-TR-202.

Othmer, D. F., and Chen, H. T., 1968, Correlating and predicting thermodynamic data: Indus. Eng. Chemistry, v. 60, no. 4, p. 39-61; reprinted in Am. Chem. Soc., Applied Thermodynamics: Washington, D.C., Am. Chem. Soc., p. 115-139.

Othmer, D. F., and Yu, E. S., 1968, Correlating vapor pressures and vapor volumes. Use of reference substance equations: Indus. Eng. Chemistry, v. 60, no. 1, p. 22-35.

Pace, K. D., 2004, Modeling and Simulation Verification and Validation challenges, Johns Hopkins apl Tchnical digest, 25, 2, 163-172.

Pan, L., WinGridder: an interactive grid generator for TOUGH2, Proceedings, TOUGH Symposium 2003, Lawrence Berkeley National Laboratory, Berkeley, California, May 12-14, 2003.

Pan, L., Oldenburg, C.M., Wu, Y. and Pruess, K., 2011, "TWell/ECO2N Version 1.0: Multiphase and Non-Isothermal Model for Coupled Wellbore-Reservoir Flow of Carbon Dioxide and Variable Salinity Water", Earth Sciences Division, Lawrence Berkeley National Laboratory, University of California, Berkeley, California 94720.

Pan, L., Oldenburg, C.M., 2013, T2Well – An integrated wellbore-reservoir simulator, Computer & Geoscience, 65, 46-55.

Pan, L., Freifeld, B., Doughty, C., Zakem, S., Sheu, M., Cutright, B., Terrail, T., 2015, Fully coupled wellbore-reservoir modelling of geothermal heat extraction using $CO_2$ as the working fluid, *Geothermics*, 53, 100-113, 2015.

Pritchett, J. W., Rice, M. H. and Riney, T. D. (1981) Equation-of-state for water-carbon dioxide mixtures: implications for Baca reservoir. Report DOE/ET/27163-8, UC-66a, La Jolla, CA, 53 pp.

Pritchett J.W. and Garg, S.K, 1995, STAR: A geothermal reservoir simulation system. Proceedings World Geothermal Congress 1995, Florence, Italy, May 18-31.

Pruess, K., 1987, TOUGH user's guide. Nuclear Regulatory Commission Rep. NUREG/CR-4645; also Lawrence Berkeley Lab. Rep. LBL-20700. Lawrence Berkeley Natl., Berkeley, CA.

Pruess, K., 1988, SHAFT, MULKOM, TOUGH: A set of numerical simulators for multiphase fluid and heat flow. Geotermia, Rev. Mex. Geoenergia 4.1, pp. 185-202.

Pruess, K., 1991, TOUGH2 - A general purpose numerical simulator for multiphase fluid and heat flow. Rep. LBL-29400. Lawrence Berkeley Natl. Lab., Berkeley, CA.

Pruess, K., Oldenburg, C., Moridis, G., 1999, TOUGH2 USER'S GUIDE, VERSION 2.0, Earth Sciences Division, Lawrence Berkeley National Laboratory, University of California, Berkeley, California 94720.

Pruess, K. and Battistelli, A., 2002, TMVOC, a Numerical Simulator for Three-Phase Non-Isothermal Flows of Multicomponent Hydrocarbon Mixtures in Saturated-Unsaturated Heterogeneous Media, Lawrence Berkeley National Laboratory Report LBNL-49375, April 2002.

Pruess K., Yabusaki S.; Steefel C., Lichtner P., 2002, Fluid Flow, Heat Transfer, and Solute Transport at Nuclear Waste Storage Tanks in the Hanford Vadose Zone. Vadose Zone Journal, Vol. 1, no. 1, p. 68-88

Pruess, K., 2004, The TOUGH Codes – A family of simulation tools for multiphase flow and transport processes in permeable media, Vadoze zone journal, vol3, 738-746.

Pruess, K., 2005, ECO2N: A TOUGH2 Fluid Property Module for Mixtures of Water, NaCl, and CO2, Report LBNL-57952, Lawrence Berkeley National Laboratory, Berkeley, Calif., 2005

Pruess, K., Oldenburg, C., Moridis, G., 2012, TOUGH2 USER'S GUIDE, VERSION 2, Earth Sciences Division, Lawrence Berkeley National Laboratory, University of California, Berkeley, California 94720, LBNL-43134.

Purwanto E.H, Kaya E. NCG-NaCl reservoir modelling in Waiotapu-Waikite-Reporoa geothermal areas. Proceedings 36th New Zealand Geothermal Workshop, 24 - 26 November 2014, Auckland, New Zealand

Ramey, H.J. Jr., Welbore heat transmission, Mobil Oil Co., Santa Fe Springs, California, 1962.

Ratouis T.M.P., O'Sullivan M.J., O'Sullivan J.P., 2016, A Numerical model of Rotorua Geothermal Field. Geothermics, 60, P. 105–125.

Rycroft, C.H, Voro++: A three-dimensional Voronoi cell library in C++, Chaos, 19, 041111, 2009.

Rutqvist, J., Wu, Y.-S., Tsang, C.-F., and Bodvarsson, G., 2002, A modeling approach for analysis of coupled multiphase fluid flow, heat transfer, and deformation in fractured porous rock, International Journal of Rock Mechanics and Mining Sciences, 39, 429-442.

Sato, T., Ohsato, K., Shiga, T., G-STAR-BASE (G*BASE). A data base system for underground information and post-processing for TOUGH2, Proceedings, TOUGH Symposium 2003, Lawrence Berkeley National Laboratory, Berkeley, California. May 12-14, 2003.

Silvester L.F., and K.S. Pitzer, 1976, Thermodynamics of geothermal brines I. Thermodynamic properties of vapor-saturated NaCl (aq) solutions from 0-300°C. Report LBL-4456, Lawrence Berkeley National Laboratory, Berkeley, Calif.

Shi H., Holmes J.A., Durlofsky L.J., Aziz K., Diaz L.R., Alkaya B., Oddie. G., 2005, Drift-flux modeling of two-phase flow in wellbores, SPR.

Sirait P., Ridwan R.H., Battistelli A., 2015,Reservoir Modeling for Development Capacity of Dieng Geothermal Field, Indonesia. Proc., Fourtieth Workshop on Geothermal Reservoir Engineering, Stanford University, Stanford, California, January 26-28, 2015.

Sutton, F. M. and McNabb, A. (1977) Boiling curves at Broadlands field. New Zealand Journal of Science 20, 333-337.

Tanaka, T., Itoi, R., Development of numerical modeling environment for TOUGH2 simulator on the basis of Graphical User Interface (GUI), Proc. of the World Geothermal Congress, Bali, Indonesia, April 25-29, 2010.

Townley, L.R., Wilson, J.L., 1980. Description of and users's manual for a finite-element aquifer flow model. In: AQUIFEM-1: Ralph M. Parsons Laboratory Technology Adaptation Program Report 79-3, 1980, Cambridge Massachusetts.

Tokita, H. and Itoi, R., 2004, Development of the MULFEWS Multi-FeedWellbore Simulator. In Proceedings of the 29th Workshop on Geothermal Reservoir Engineering Stanford University, Stanford, California, USA.

Vasini, E.M., Battistelli, A., Berry, P., Bonduà, S., Bortolotti, V., Cormio, C., Pan, L., 2015, Interpretation of production tests in geothermal wells with T2Well-EWASG, Proceedings of the TOUGH Symposium 2015, LBNL, Berkeley, California, September 28-30.

Vatnaskil Consulting engineers:
http://www.vatnaskil.is/softwaredevelopment.html

Vinsome, P.K.W. and Shook, G.M., 1993, Multi-purpose simulation, Journal of Petroleum Science and Engineering, 9(1), 29-38.

Voronoi G., 1908, Nouvelles applications des paramètres continus à la théorie des formes quadratiques. Deuxième mémoire. Recherches sur les paralléllοèdres primitifs, Journal für die reine und angewandte Mathematik, volume 134, pag. 198-287.

Weisbrod, N., Pillersdorf, M., Dragila, M., Graham, C., Cassidy, J. and Cooper, C. A., 2005. Evaporation from Fractures Exposed at the Land Surface: Impact of Gas-Phase Convection on Salt Accumulation, in Dynamics of Fluids and Transport in Fractured Rock (eds B. Faybishenko, P. A. Witherspoon and J. Gale), American Geophysical Union, Washington, D. C.

Wellmann, J.F., Croucher, A., Regenauer-Lieb, K., Python scripting libraries for subsurface fluid and heat flow simulations with TOUGH2 and SHEMAT, Comput. Geosci. 43, 197-206, 2012.

Willhite G.P, 1967, Pverwall Heat transfer coefficents in steam and hot water injection wells, Continental Oil Co. Ponca City Okla, May, 1967.

Xu, T., Pruess, K., 2001. Modelling multiphase non-isothermal fluid flow and reactive geochemical transport in variably saturated fractured rocks: 1 methodology. American Journal of Science, vol.301, 16-33, 2001.

Xu, T., Sonnenthal, E., Spycher, N., and Pruess, K., 2004. TOUGHREACT User's guide: a simulation program for non-isothermal multiphase reactive geochemical transport in variably saturated geologic media. Earth Science Division, Lawrence Berkeley National Laboratory, University of California, Berkeley, CA 94720.

Zhang, K., Wu, Y.S., and Pruess, K., 2008, User's Guide for TOUGH2-MP – A Massively Parallel Version of the TOUGH2 Code, Earth Science Division, Lawrence Berkeley National Laboratory, LBNL-315E.

Zhang, Y., Pan, L., Pruess, K., Finsterle, S., A time-convolution approach for modeling heat exchange between a wellbore and surrounding formation, *Geothermics*, 40, 4, 261-266, 2011.

Zhang, J., Xing, H., Numerical modelling of non-Darcy flow in near-well region of a geothermal reservoir, Geothermics, 42, 78-86, 2012.

Zuber, N., Findlay, J.A., Average volumetric concentration in two-phase flow systems, *Journal of Heat Transfer*, 87, 453, 1965.